

https://doi.org/10.1093/petrology/egac032
Original Manuscript

Distinguishing Volcanic Contributions to the Overlapping Samoan and Cook-Austral Hotspot Tracks

Allison A. Price^{1,*}, Matthew G. Jackson¹, Janne Blichert-Toft², Kevin Konrad³, Michael Bizimis⁴, Anthony A.P. Koppers⁵, Jasper G. Konter⁶, Valerie A. Finlayson⁷ and John M. Sinton⁶

- ¹Department of Earth Science, University of California, Santa Barbara, Santa Barbara, CA 93106, USA
- ²Ecole Normale Supérieure de Lyon, CNRS, Université de Lyon, 69007 Lyon, France
- ³Department of Geoscience, University of Nevada Las Vegas, Las Vegas, NV 89154, USA
- ⁴School of Earth, Ocean and Environment, University of South Carolina, Columbia, SC 29208, USA
- ⁵College of Earth, Ocean and Atmospheric Sciences, Oregon State University, Corvallis, OR 97331, USA
- Department of Earth Sciences, School of Ocean and Earth Science and Technology, University of Hawai'i Manoa, Honolulu, HI 96822, USA
- ⁷Department of Geology, University of Maryland College Park, College Park, MD 20742, USA

Abstract

To deconvolve contributions from the four overlapping hotspots that form the "hotspot highway" on the Pacific plate—Samoa, Rarotonga, Arago-Rurutu, and Macdonald—we geochemically characterize and/or date (by the 40 År/39 Ar method) a suite of lavas sampled from the eastern region of the Samoan hotspot and the region "downstream" of the Samoan hotspot track. We find that Papatua seamount, located \sim 60 km south of the axis of the Samoan hotspot track, has lavas with both a HIMU (high $\mu=^{238}$ U/ 204 Pb) composition (206 Pb/ 204 Pb = 20.0), previously linked to one of the Cook-Austral hotspots, and an enriched mantle I (EM1) composition, which we interpret to be rejuvenated and Samoan in origin. We show that these EM1 rejuvenated lavas at Papatua are geochemically similar to rejuvenated volcanism on Samoan volcanoes and suggest that flexural uplift, caused by tectonic forces associated with the nearby Tonga trench, triggered a new episode of melting of Samoan mantle material that had previously flattened and spread laterally along the base of the Pacific plate under Papatua, resulting in volcanism that capped the previous HIMU edifice. We argue that this process generated Samoan rejuvenated volcanism on the older Cook-Austral volcano of Papatua. We also study Waterwitch seamount, located \sim 820 km WNW of the Samoan hotspot, and provide an age (10.49 \pm 0.09 Ma) that places it on the Samoan hotspot trend, showing that it is genetically Samoan and not related to the Cook-Austral hotspots as previously suggested. Consequently, with the possible exception of the HIMU stage of Papatua seamount, there are currently no known Arago-Rurutu plume-derived lava flows sampled along the swath of Pacific seafloor that stretches between Rose seamount (~25 Ma) and East Niulakita seamount (~45 Ma). located 1400 km to the west. The "missing" ~20-million-year segment of the Arago-Rurutu hotspot track may have been subducted into the northern Tonga trench, or perhaps was covered by subsequent volcanism from the overlapping Samoan hotspot, and has thus eluded sampling. Finally, we explore tectonic reactivation as a cause for anomalously young volcanism present within the western end of the Samoan hotspot track.

Keywords: radiogenic isotopes, geochemistry, OIB, Samoa, Cook-Austral

INTRODUCTION

Hotspots are generally thought to be formed by upwelling mantle plumes that melt beneath an overriding plate. This mechanism produces a hotspot track, a series of age-progressive volcanoes that extend linearly away from the volcanically active hotspot (e.g. Morgan, 1971, 1972). The so-called "hotspot highway" in the south Pacific results from four overlapping hotspot tracks—Macdonald, Arago-Rurutu, Rarotonga, and Samoa—that lie on the same Pacific plate flowline (e.g. Duncan & McDougall, 1976; Turner & Jarrard, 1982; Matsuda et al., 1984; Diraison, 1991; Chauvel et al., 1997; McNutt et al., 1997; Bonneville et al., 2002; Bonneville et al., 2006; Konter

et al., 2008; Jackson et al., 2010; Maury et al., 2013; Finlayson et al., 2018; Jackson et al., 2020; Buff et al., 2021) (Fig. 1). The "downstream" Samoan hotspot track in the hotspot highway is anchored on the young end by the volcanically active Vailulu'u seamount and extends toward older volcanoes in the west that reach ages of ~24 Ma (Figs 1 and 2). The Samoan hotspot track is divided into two provinces: (1) the Eastern Samoan Volcanic Province (ESAM), which is bracketed on the east end by the volcanically active Vailulu'u seamount and extends ~350 km to the west to Savai'i (5.29 Ma; Koppers et al., 2008) (Hart et al., 2000; Staudigel et al., 2004, 2006); and (2) the Western Samoan Volcanic Province (WESAM), which

^{*}Corresponding author. E-mail: price@ucsb.edu

consists of older Samoan volcanoes that lie to the west of Savai'i and extend westward to Alexa bank (23.96 Ma; Hart et al., 2004), located ~1300 km west of Savai'i Island (e.g. Hawkins & Natland, 1975; Duncan, 1985; Sinton et al., 1985; Johnson et al., 1986; Jackson et al., 2010) (Figs 1 and 2). Samoan lavas can exhibit high ³He/⁴He signatures, up to 34 R_A (where R_A is the measured ratio relative to atmosphere; Jackson et al., 2007a) or strong enriched mantle II (EM2) compositions characterized by high 87 Sr/ 86 Sr (up to 0.723888 \pm 0.000015 [2SE] in magmatic clinopyroxene; Adams et al., 2021), although we note that high ³He/⁴He and high ⁸⁷Sr/⁸⁶Sr are not found in the same samples (e.g. Jackson et al., 2007a). Samoan lavas can also exhibit geochemical characteristics that are associated with dilute contributions from three other canonical mantle endmembers—enriched mantle I (EM1), HIMU (high $\mu = {}^{238}\text{U}/{}^{204}\text{Pb}$), and a depleted component (DM) (e.g. Jackson et al., 2014).

Along the Samoan hotspot track, several volcanoes occur "off axis" and are displaced to the south of the main hotspot trace. For example, Papatua seamount is located ~60 km south of the Samoan island of Tutuila. Jackson et al. (2010) presented data for a Papatua lava (sample ALIA-D129-05, dredged at 2518-2408 meters below sea level (mbsl)) with a HIMU geochemical composition, which they interpreted to be of non-Samoan origin and potentially related to one of the Cook-Austral hotspots. They argued that the HIMU flavor in this lava, along with the thick (>5 cm) ferromanganese rind attached to the Papatua sample (which contrasts with the thin [<1 mm] ferromanganese patinas on submarine samples from nearby Samoan volcanoes), is evidence that Papatua was erupted over one of the HIMU Cook-Austral hotspots that lie ~2200 km (Arago-Rurutu hotspot) to ~3400 km (Macdonald hotspot) ESE of the Samoan hotspot. In support of this hypothesis, volcanic seamounts comprising older portions of the Cook-Austral hotspot tracks have been found in the vicinity of the Samoan hotspot track. For example, Rose atoll (24.8 ± 1 Ma; Buff et al., 2021), located adjacent to Vailulu'u seamount, relates to the Arago-Rurutu hotspot (Figs 1 and 2). Malulu seamount, which lies between Rose atoll and Vailulu'u seamount (Figs 1 and 2), has a HIMU composition and therefore likely relates to either the Arago-Rurutu or Macdonald hotspot (but ages are not available for Malulu, hence a specific designation cannot be made; Buff et al., 2021). Located ~350 km north of Vailulu'u, the HIMU Moki seamount (44.53 \pm 10.05 Ma; Buff et al., 2021) relates to the Macdonald hotspot (Figs 1 and 2). At the older end of the Samoan hotspot track, East Niulakita seamount has been shown to host both older HIMU Arago-Rurutu lavas $(42.24 \pm 0.82 \text{ Ma}-45.73 \pm 0.14 \text{ Ma};$ Finlayson et al., 2018) and younger shield-stage Samoan lavas $(14.76 \pm 0.12 \text{ Ma}; \text{Finlayson et al., 2018})$ (Figs 1 and 2). It is evident that volcanoes in the Samoan region must be distinguished by age and/or geochemical composition to determine their hotspot of origin, as Cook-Austral hotspot volcanoes in the Samoan region have older ages

and different geochemical compositions than Samoan hotspot volcanoes.

Here we report geochemical and isotopic data and ⁴⁰Ar/³⁹Ar ages on selected lavas from eight submarine volcanoes located in the Samoan region: the dataset includes 12 lavas from seven volcanoes in the WESAM region (including new 40 Ar/39 Ar ages on four samples), as well as geochemical data on two glasses from Papatua seamount. Using the data, we explore three significant findings: first, we evaluate whether old volcanoes from the Cook-Austral hotspots can be traced into the WESAM region of the Samoan hotspot track. Second, we investigate the origins of the two stages of volcanism at Papatua seamount. Lastly, we examine the causes of rejuvenated volcanism at Papatua and along the WESAM portion of the Samoan hotspot.

Sample location and descriptions

The samples in this study were recovered during four separate dredging expeditions: samples with prefix KK8203 were collected during the 1982 KK820316 cruise of the R/V Kana Keoki; samples with prefix PPT were collected during the 1986 Papatua Expedition of the R/V Thomas Washington; one sample with prefix ALIA was collected by seafloor dredging during a 2005 expedition of the R/V Kilo Moana; samples with prefix RR1310 were recovered by seafloor dredging during a 2013 expedition of the R/V Roger Revelle. The volcanoes sampled (and presented in this study) include the Lalla Rookh, Siafiafi, Bustard, Waterwitch, Talviuni, Fa'aitu, and Papatua seamounts and Tuscarora bank (Fig. 2). Only basalt clasts hosted in hyaloclastite were obtained from Lalla Rookh (RR1310-D40-10), Siafiafi (ALIA-D121-09), Tuscarora (KK8203-DR-9), and Talviuni (KK8203-DR-1); in these cases, only the freshest clasts were separated for geochemical and isotopic analyses. In total, 14 volcanic samples from eight different volcanoes were geochemically and isotopically characterized and/or dated by the 40 Ar/ 39 Ar method.

Table 1 provides sample descriptions and locations, information about which samples have new 40 Ar/39 Ar ages, major and trace element, and/or isotope data, as well as information about prior isotopic studies of samples from the same volcanoes.

METHODS

⁴⁰Ar/³⁹Ar age determination

New 40 Ar/39 Ar age determinations on four submarine lava flows are presented in Table 2. Three plagioclase separates and two groundmass separates were obtained by systematic crushing, sieving, magnetic separation, acid leaching, and handpicking as described in Konrad et al. (2018). Samples were irradiated along with Fish Canyon Tuff (FCT) sanidine fluence monitors at the Oregon State University TRIGA reactor for 6 h. Extracted gas was analyzed using an ARGUS VI mass

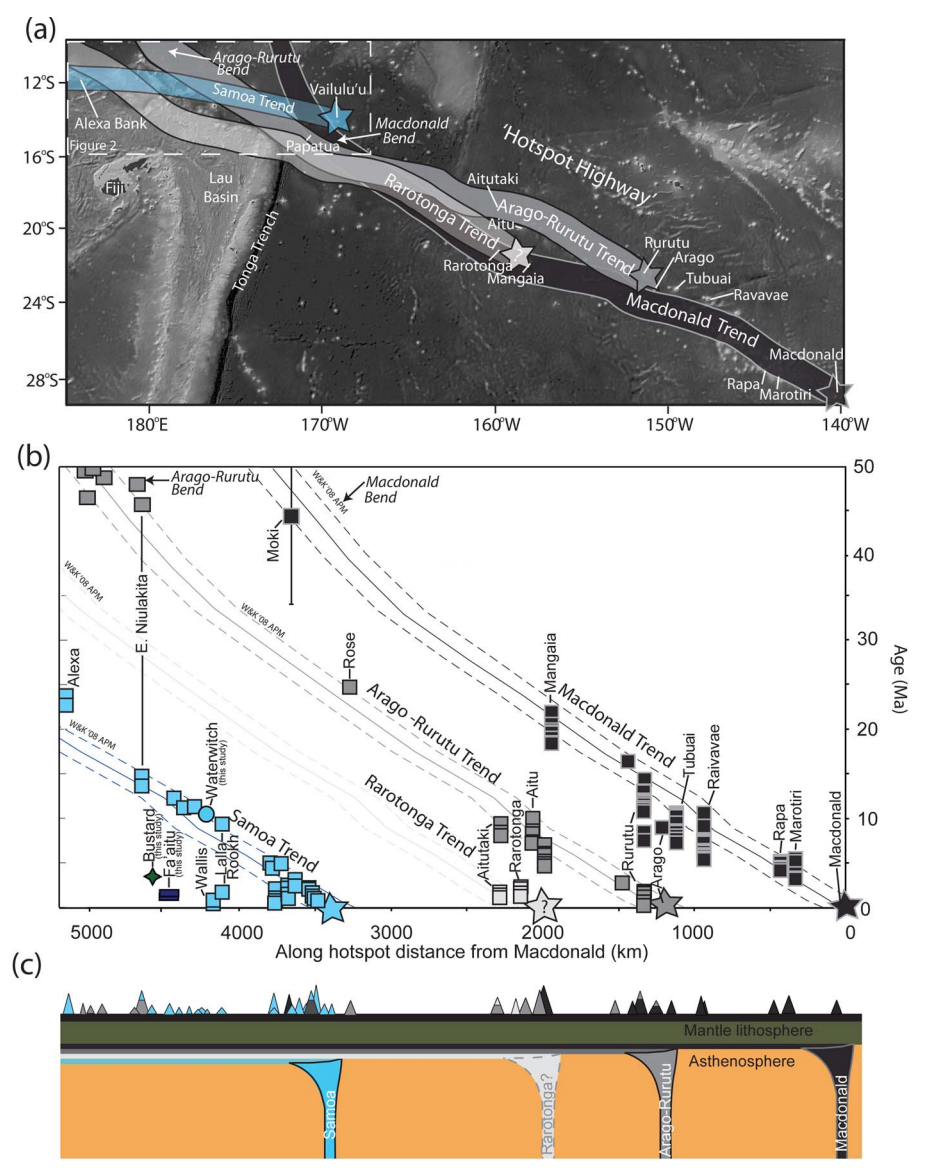


Fig. 1. Hotspot reconstruction, age progression, and cross section. Panel (a) shows the Samoan trend and the Cook-Austral hotspot tracks (Macdonald, Arago-Rurutu, and Rarotonga) consistent with the Wessel & Kroenke (2008) absolute plate motion model. The locations of the active hotspots are marked with stars. The location of the Rarotonga hotspot, if it exists, remains to be discovered and is shown as a star with a question mark. Panel (b) shows the age progression for the Macdonald, Arago-Rurutu, Rarotonga, and Samoa hotspot tracks based on Wessel & Kroenke (2008) (WK08 APM); ages for the Cook-Austral volcanoes are summarized in Jackson et al. (2020) and Buff et al. (2021), while Samoan ages are summarized in Koppers et al. (2008). New ages for Waterwitch, Fa'aitu, and Bustard seamounts are also shown: Waterwitch clearly lies on the Samoan hotspot age progression, and Fa'aitu and Bustard do not (but could represent rejuvenated volcanism). Panel (c) shows a cartoon cross section that links volcanoes from the age-distance plot (panel b) to their respective hotspot (note color coding in both panels). Volcanoes with two known stages of volcanism (e.g. Rurutu, Arago, Aitutaki, Papatua, and East Niulakita) are represented by two colors on a single volcano with the bottom color relating to the first stage of volcanism and the top color relating to the second stage. The older stage of Papatua is shown in a medium gray as we are currently unable to determine if this HIMU stage is related to the Macdonald hotspot or the Arago-Rurutu hotspot. Location of the sampled region in Fig. 2 is shown in panel (a). The equivalent HEB (Hawaii-Emperor Bend) locations for the Macdonald and Arago-Rurutu hotspots are marked on the map (a) and age-distance figure (b).

spectrometer. Samples were analyzed via the incremental heating method using 21-27 CO₂ laser heating steps with blanks analyzed at the start, end, and between every three heating steps. Age determinations were calculated using ArArCALC v2.7.0 (Koppers, 2002) with an FCT age of 28.201 ± 0.046 Ma (Kuiper et al., 2008) and the decay constant of Min et al. (2000). Ages were considered reliable if plateau lengths were greater than 60% of the ³⁹Ar released and probability of fit factors were > 5%. A sample with a plateau consisting of 40-60% of ³⁹Ar released is considered a mini-plateau, and we interpret the corresponding age with caution.

Major and trace elements

Major element analyses of whole rock powders were conducted at Washington State University (WSU) by Xray fluorescence (XRF) spectrometry on a ThermoARL XRF following methods outlined elsewhere (Johnson & Sinton, 1990). The USGS BCR-2 reference material was run together with the samples. Measured major element

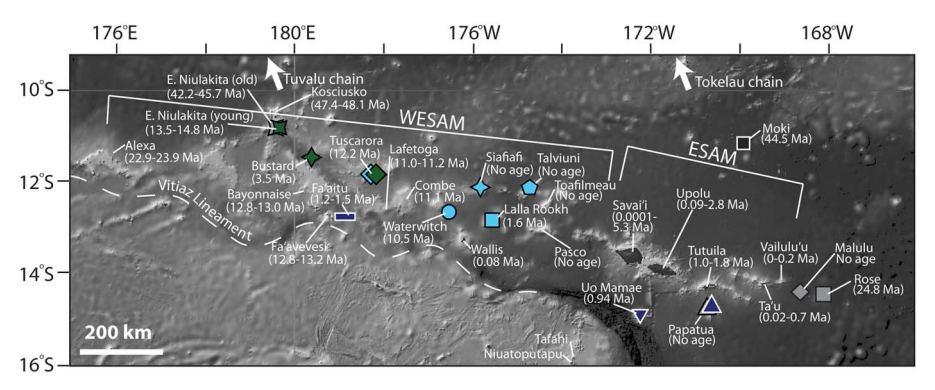


Fig. 2. Map of the study region including sample locations and other important volcanoes and geologic features. Volcanoes characterized in this study, and important volcanoes mentioned in the text, are marked with symbols, which are used in successive figures. Ages below each volcano are in millions of years and represent the youngest and oldest lavas from that volcanoes with only one dated lava have a single age, while volcanoes marked with "no age" have no published age. Ages are from this study, Hawkins & Natland (1975), Price et al. (1991), Hart et al. (2004), Koppers et al. (2008, 2011), McDougall (2010), Finlayson et al. (2018), Konrad et al. (2018), and Buff et al. (2021). Base map was created using GeoMapApp (http://www. geomapapp.org) with topographic and bathymetric data from SRTM_PLUS (Becker et al., 2009). WESAM (western Samoa) and ESAM (eastern Samoa) regions are shown.

concentrations for the BCR-2 analyzed here are within 1.8% of the recommended values in Jochum et al. (2016), except for P₂O₅ (3.7%), and the data are reported in Table 3. Six samples from this study—RR1310-D40-10, RR1310-D34-01, KK8203-DR-1, KK8203-DR-9, ALIA-D121-09, and RR1310-D29-01—were not measured for major element concentrations, generally owing to lack of suf-

Major elements of Papatua glasses (PPT-D1-N1 and PPT-D1-N2) were measured in situ by electron microprobe at UC Santa Barbara (UCSB) using primary standards and following the analytical conditions outlined in Jackson et al. (2015). The secondary MORB glass standard ALV519-4-1 was measured repeatedly throughout the analytical session (Table 4). The replicate major element analyses of ALV519-4-1 are reproducible to within 2.0% (2RSD, N = 22) except for Na₂O (2.5%), K₂O (4.5%), MnO (5.2%), and P_2O_5 (19%), while the major element concentrations of ALV519-4-1 reported here agree with the Melson et al. (2002) values to within 3.2% except for K_2O (18.7%) and P₂O₅ (27.1%) (the low concentrations of these two elements, at \sim 0.1 wt %, may explain the poorer agreement).

Trace element analyses on all samples, except the two Papatua glasses, were measured by ICP-MS at WSU on ~200 mg of whole-rock or hyaloclastite clast powder. Methods followed those described elsewhere (Knaack et al., 1994; Hart & Blusztajn, 2006). An aliquot of the USGS BCR-2 reference material was run as an unknown together with the samples to assess reproducibility. Measured trace element concentrations are within 6.8% of the recommended values in Jochum et al. (2016), except for Eu (7.1%), Tb (9.5%), Dy (8.8%), and Ho (11.4%) (Table 3). Three samples from this study, RR1310-D40-10, RR1310-D34-01, and RR1310-D29-01, were not measured for trace element concentrations.

Trace element analyses on the two Papatua glasses (PPT-D1-N1 and PPT-D1-N2) were measured using a Thermo Scientific Element XR ICP-MS coupled to a Resonetics M-50E 193 nm ArF excimer laser at Laboratoire

Magmas et Volcans at Clermont-Ferrand. Samples were internally standardized using ⁴³Ca. Analytical methods followed those in Oulton et al. (2016) and Reinhard et al. (2018) except that a 47- μ m laser spot fired with a 4 Hz repetition rate was used for analysis of both samples and standards. Calibration curves were generated using the NIST612 (Gagnon et al., 2008) and BCR-2 (Jochum et al., 2006) glasses. Replicate analyses of the MORB glass standard ALV519-4-1 were made throughout the analytical session to monitor and evaluate precision and accuracy. The reproducibility of the trace element analyses was better than 6.1% (2RSD, N = 8) for all elements, except for U (6.9%), Pb (9.9%), Ta (7.3%), and Cs (44%). Measured concentrations are compared with previously published analyses from Melson et al. (2002) and Gale et al. (2013a, 2013b) in Table 4.

Hafnium, Nd, Sr, and Pb chemical separation and mass spectrometry

The radiogenic isotopic data presented here were measured during two analytical campaigns: the first at the Ecole Normale Supérieure de Lyon (ENS Lyon) and University of North Carolina Chapel Hill (UNC) and the second at UCSB and University of South Carolina (USC) (Table 5).

Analyses carried out at ENS Lyon and UNC

Isotopic compositions were measured on ~200 mg of handpicked rock chips (not powders), except for the two Papatua samples for which isotopic compositions were measured on glasses. All samples were leached and dissolved at ENS Lyon using an aggressive leaching method described in Price et al. (2016), except for the Papatua glasses, which were subjected to a lighter leach (see method described in Blichert-Toft & Albarède (2009) and Price et al. (2014)). In short, the aggressive leaching procedure first included a leach in 1 ml 30% Suprapur H₂O₂ for 15 min at 130 °C, a 15 min ultrasonication step, and an additional 10 min of heating at 130 °C. The H_2O_2 was pipetted off and the samples rinsed twice with MilliQ

Downloaded from https://academic.oup.com/petrology/article/63/5/egac032/6563380 by University of California, Santa Barbara user on 05 June 2022

Table 1. Sample descriptions¹

Sample name	Location	Lat	Lon	WESAM or ESAM	Rock description	Prev. publ. isotopic data from same volcano?	Isotopic data in this study	Major element data in this study	Trace element data in this study	40Ar/39Ar age in this study
PPT-D1-N1 glass	Papatua	-14.77	-170.67	ESAM	Fresh pillow glass attached to peridotite xenolith	Yes, Jackson et al. (2010) (ALIA-DR129-05); xenoliths analyzed by Poreda & Farley (1992)	Yes	Yes	Yes	o N
PPT-D1-N2 glass	Papatua	-14.77	-170.67	ESAM	Fresh pillow glass attached to peridotite xenolith	Yes; Jackson et al. (2010) (ALIA-DR129-05); xenoliths analyzed by Poreda & Farley (1992)	Yes	Yes	Yes	o N
RR1310-D41-05	Lalla Rookh	-12.92	-175.39	WESAM	Fresh aphanitic basalt	Yes; Hart et al. (2004) (KK820316 3-26, 3-36, and 3-43)	Yes	Yes	Yes	o Z
RR1310-D40-10 clast	Lalla Rookh	-12.65	-175.41	WESAM	Four ~2 cm clasts of visually altered basaltic material separated from hyaloclastite; clasts were visually similar lithology and were combined for analysis due to limited material	Yes; Hart et al. (2004) (KK820316 3-26, 3-36, and 3-43)	Yes	o Z	o N	o Z
RR1310-D39-01	Siafiafi	-12.30	-176.06	WESAM	Fresh aphanitic basalt	Yes; clinopyroxene separate from Jackson et al. (2010) (ALTA-DR121-09)	Yes	Yes	Yes	o
ALIA-D121-09 clast	Siafiafi	-12.33	-175.75	WESAM	Visually altered basaltic clast picked from hyaloclastite	Yes; clinopyroxene separate from Jackson et al. (2010) (ALIA-DR121-09)	Yes	o _N	Yes	o N
RR1310-D29-01 RR1310-D29-10 RR1310-D34-01	Bustard Bustard Tuscarora	-11.52 -11.52 -11.98	-179.70 -179.70 -178.27	WESAM WESAM WESAM	Fresh alkali basalt Fresh vesicular pillow basalt A small (~3 cm) piece of fresh	No No Yes; Finlayson et al. (2018)	No Yes Yes	No Yes No	No Yes No	Yes No No
KK8203-DR-9 clast	Tuscarora	-11.85	-177.88	WESAM	basaltic spatter Multiple small (<1 cm), lithologically similar clasts of basalt picked from hyaloclastite; the clasts were visually similar in lithology and were combined for analysis due to limited	(RR1310-D33-32) Yes; Finlayson et al. (2018) (RR1310-D33-32)	Yes	o Z	Yes	o Z
RR1310-D38-08	Waterwitch	-12.78	-176.50	WESAM	nateriar Lightly altered basalt	Yes; Jackson et al. (2010) (ALIA-DR122-03)	Yes	Yes	Yes	Yes
KK8203-DR-1 clast	Talviuni	-12.27	-174.63	WESAM	Visually altered vesicular basaltic clast picked from hyaloclastite	No	Yes	No	Yes	oN N
RR1310-D31-01 RR1310-D31-02	Fa'aitu Fa'aitu	-12.79 -12.79	-178.88 -178.88	WESAM WESAM	Fresh plagioclase ultraphyric basalt Fresh plagioclase ultraphyric basalt	No No	Yes	Yes	Yes	Yes

¹The amount of material limited the types of analyses that were carried out for some of the samples in this study. Isotopic, major, and trace element data are available only for the largest samples. Samples with only isotopic and trace element data are from smaller samples. The smallest samples only have isotopic data. Due to visible alteration for some of the samples in this study, an intensive leaching procedure was applied to all but two samples prior to dissolution and chemistry, the Papatua glasses were subjected to less intensive leaching.

Fable 2. 40 Ar/39 Ar ages

Samp	Sample information					Pla	Plateau							Inve	Inverse isochron		
Sample name Material Seamount	Material	Seamount	Age	Age \pm 2S (i)	\pm 2S (f) 39 Ar K/Ca	³⁹ Ar	K/Ca	± 2S	\pm 2S MSWD P n N	Ъ	u	Age	± 2S (i)	± 2S (f)	\pm 2S (i) \pm 2S (f) 40 Ar/ 36 Ar intercept \pm 2S	± 2S	SF
RR1310-D29-01 * Groundmass	Groundmass	Bustard	3.47	3.47 ±0.02Ma	± 0.08Ma	41%	0.124	±0.003		53%	7		±0.09Ma	± 0.12Ma	273.14	±129.73	3%
RR1310-D31-01	Plagioclase	Fa'atiu	1.26	±0.14Ma	± 0.14Ma	100%	0.005	±0.000		81%	22 '		±0.16Ma	\pm 0.16Ma	290.88	±9.81	20%
RR1310-D31-02	Plagioclase	Fa'atiu	1.48	$\pm 0.19~\mathrm{Ma}$	± 0.19Ma	%06	0.005	±0.000	0.49	%/6	97% 20 24	1.51 ±	±0.21Ma	± 0.21 Ma	289.34	± 21.82	28%
RR1310-D38-08	Plagioclase	Waterwitch	10.49	±0.09Ма	± 0.25Ma	%29	0.014	±0.000		84%	14 2		±0.24Ma	± 0.34Ma	298.56	± 31.34	16%
RR1310-D38-41	Plagioclase	Waterwitch	N/A														

f = full uncertainty; i = internal uncertainty; MSWD = Mean square of weighted Summary of 40 Ar/39 Ar age analysis on five groundmass and/or plagioclases from dredges RR1310-D29, RR1310-D31, and RR1310-D38. f = full uncertainty; i = internal uncertainty; MS\ deviations; P = probability of fit, n = steps used in age calculation; N = total steps; SF = spreading factor; * indicates the age is a mini plateau and should be interpreted with caution. H₂O. The samples were then leached in 2 ml distilled 6 M HCl for 1 h at 130 °C, followed by 10 min of ultrasonication and 10 further min of heating at 130 °C. The HCl was pipetted off, and the samples were rinsed twice with MilliQ H2O. Lastly, the samples were leached in 2 ml distilled 4 M HNO₃ for 1 h at 130 °C, followed by 15 min of ultrasonication and 10 additional min of heating at 130 °C. The HNO₃ was pipetted off and the samples rinsed twice with MilliQ H₂O. In contrast, the light leach consisted of leaching glass chips in 2 ml distilled 6 M HCl for a total of 50 min at 120 °C, including several intermittent steps of ultrasonication. The HCl was pipetted off and the samples rinsed twice with MilliQ H2O.

Following sample dissolution in concentrated distilled HF and HNO₃ in the ratio of \sim 3:1, Hf and Pb were separated by column chromatography at ENS Lyon according to the protocols outlined in Blichert-Toft et al. (1997) and Blichert-Toft & Albarède (2009) and measured by MC-ICP-MS (Nu Plasma 500 HR), also at ENS Lyon. Lead isotopic compositions were corrected for instrumental mass fractionation by Tl addition (using a 205 Tl/203 Tl ratio of 2.38890) assuming an exponential fractionation law. The measured Pb isotopic compositions were further corrected to the NIST 981 values of Eisele et al. (2003) $(^{206}\text{Pb}/^{204}\text{Pb} = 16.9409 \pm 19, ^{207}\text{Pb}/^{204}\text{Pb} = 15.4976 \pm 24, \text{ and}$ 208 Pb/ 204 Pb = 36.7262 ± 86 (2 σ)) using sample-standard bracketing with NIST 981 being analyzed systematically every second sample throughout the run sessions. Instrumental mass fractionation correction of the measured Hf isotopic ratios also assumed an exponential fractionation law and a ¹⁷⁹Hf/¹⁷⁷Hf ratio of 0.7325. The unweighted mean ¹⁷⁶Hf/¹⁷⁷Hf of the JMC-475 Hf standard, which was run alternately with the samples, was identical within error to the preferred value of 0.282163 ± 0.000009 (Blichert-Toft et al., 1997); hence, no further corrections were applied to the ¹⁷⁶Hf/¹⁷⁷Hf data obtained in this study. The wash from the Pb columns containing the Sr and Nd fractions was collected in clean Savillex beakers and dried down, then redissolved and split into two fractions at UNC to be measured for Sr and Nd isotopes.

Strontium purification was carried out at UNC by column chromatography and Sr isotopic compositions measured on a VG Sector 54 TIMS using the same methods as outlined in Jackson et al. (2017). Instrumental mass fractionation correction assumed an exponential fractionation law and a 86 Sr/88 Sr ratio of 0.1194. NBS987 run during the analysis of unknowns averaged 0.710256 ± 0.000013 (2 SD, N = 4), and the Sr isotopic compositions of all lavas are corrected for the offset between measured ⁸⁷Sr/⁸⁶Sr and preferred ⁸⁷Sr/⁸⁶Sr (0.710240) from each analytical session. Neodymium separations were also carried out at UNC and Nd isotopic compositions measured as oxides on a PhoeniX TIMS following methods outlined in Jackson et al. (2017). Correction for instrumental mass fractionation assumed an exponential fractionation law and a 146 Nd/ 144 Nd ratio of 0.7219. All samples were corrected for the offset between measured

Downloaded from https://academic.oup.com/petrology/article/63/5/egac032/6563380 by University of California, Santa Barbara user on 05 June 2022

Table 3. Major and trace element analyses of lavas examined in this study

Sample name	a.	RR1310- D29-10	RR1310- D31-01	RR1310- D31-02	RR1310- D38-08	RR1310- D39-01	RR1310- D41-05	KK8203- DR-1	KK8203- DR-9	ALIA- D121-09	BCR-2	Preferred BGR-2 (Jochum et al., 2016)
Volcano		Bustard	Fa'aitu	Fa'aitu	Waterwitch	Siafiafi	Lalla Rookh	Talviuni	Tuscarora	Siafiafi		
Material analyzed		Whole rock powder	Whole rock powder	Whole rock powder	Whole rock powder	Whole rock powder						
Method of major element analysis	nt analysis	${ m XRF}^1$	${ m XRF}^1$	XRF^1	${ m XRF}^1$	${ m XRF}^1$	XRF^1	1	1	-	XRF^1	I
Method of trace element analysis	ıt analysis	XRF, solution ICP ²	Solution ICP ²	Solution ICP ²	Solution ICP ²	Solution ICP ²	I					
XRF majors												
SiO ₂	(wt %)	45.34	50.00	50.19	47.26	57.08	45.28	I	I	I	54.30	54.93
TiO2	(wt %)	2.46	1.91	1.90	4.01	0.30	2.70	1	I	1	2.29	2.30
Al_2O_3	(wt %)	15.27	17.18	16.94	13.68	18.80	9.92			1	13.54	13.71
FeOtot	(wt %)	8.42	9.38	9.33	12.79	2.54	11.38				12.47	12.61
MnO	(wt %)	0.15	0.14	0.14	0.17	0.25	0.17	1	1		0.20	0.20
MgO	(wt %)	9.02	5.17	5.75	5.90	0.92	13.11	I			3.60	3.66
CaO	(wt %)	9.10	11.14	10.93	10.66	1.21	10.19				7.15	7.24
Na ₂ O	(wt %)	4.06	2.91	2.86	2.68	6.04	1.74		l	l	3.18	3.17
N2U	(WL %)	72.7	0.80 0.00	0.88	0.84	6.29	1.47				1.80	1.8U
101%	(wt %)	1.79	0.23	0.23	7.05	60.0 197	3 11) (-)
Total (maiors only) ³	(wt %)	97.33	98.97	99.16	98.45	93.51	96.47				98.86	
Total (majors + trace	(wt %)	99.73	99.81	99.74	99.75	99.91	76.96	1	I	I		Ι
oxides $+ LOI$ ³												
XRF traces (RR1310 samples only)	ples only)											
N:	(mdd)	185	50.8	6.79	82.5	21.4	451	1	1	1		1
Cr	(mdd)	246	212	201	71.4	3.6	699	1	I	I		1
	(mdd)	21.6	25.9	25.9	32.7	0.4	23.0	1	I		l	I
	(mdd)	184	236	233	391	7.7	241	1	1	1		I
	(mdd)	710	140	137	174	318	383					1
Rb (p	(mdd)	73.6	16.4	16.6	16.9	116	38.1	1	I	I	I	1
	(mdd)	924	379	368	426	301	489	1	I	I		I
Zr (p	(mdd)	249	137	137	239	1032	215	1	I	1	ļ	1
	(mdd)	24.1	21.7	21.0	34.8	35.6	24.2	1	I	I	I	1
	(mdd)	84.9	16.4	17.2	33.9	203	54.4					1
	(mdd)	18.3	20.8	21.6	22.2	28.7	18.2		I	1		1
	(mdd)	45.8	39.9	42.7	108	10.2	85.9	1				1
d) uz	(mdd)	72.5	93.5	92.3	134	200	120		I		l	I
												(Continued)

Downloaded from https://academic.oup.com/petrology/article/63/5/egac032/6563380 by University of California, Santa Barbara user on 05 June 2022

Table 3. Continued

lable 3. Collulined	מט											
Sample name	name	RR1310- D29-10	RR1310- D31-01	RR1310- D31-02	RR1310- D38-08	RR1310- D39-01	RR1310- D41-05	KK8203- DR-1	KK8203- DR-9	ALIA- D121-09	BCR-2	Preferred BCR-2 (Jochum et al., 2016)
Pb	(mdd)	6.2	2.1	2.2	2.8	13.8	4.7	ı	ı		ı	
La	(mdd)	57.3	14.8	14.6	28.5	200	50.2	1	I	1	I	I
Ce	(mdd)	108	32.3	34.0	62.6	336	101		I			I
Th	(mdd)	9.7	2.1	1.3	3.0	24.8	6.3	1	I	I	I	I
Nd	(mdd)	42.7	16.8	19.7	36.0	8.66	46.1					I
Ω	(mdd)	3.8	2.3	0.5	1.3	1.6	3.0	I	I		I	l
Solution ICP traces (RR1310, KK8203, ALIA, and BCR-2)	(RR1310, KK8203,	, ALIA, and BC	R-2)									
Cs	(mdd)	1.2	0.2	0.2	0.3	0.2	9.0	0.5	0.2	0.4	1.1	1.2
Rb	(mdd)	74.0	14.4	15.2	16.0	116.7	38.2	26.5	10.0	28.4	46.5	46.0
Ba	(mdd)	704	133	129	163	322	373	380	38	254	683	684
Th	(mdd)	10.3	1.8	1.8	2.9	26.1	6.2	8.6	1.1	5.4	6.2	5.8
Ω	(mdd)	2.4	0.5	0.5	8.0	1.3	1.2	1.2	0.5	1.0	1.7	1.7
Nb	(mdd)	85.5	17.1	17.1	34.8	204	55.1	98.9	10.2	57.6	11.6	12.4
Ta	(mdd)	5.4	1.2	1.2	2.4	11.3	3.3	6.8	0.7	4.0	0.8	0.8
La	(mdd)	9.09	15.0	14.8	27.2	206.5	48.1	0.69	6.3	68.7	25.7	25.1
Ce	(mdd)	107	32.9	33.0	62.0	349	97.4	136.1	12.8	126	53.5	53.1
Pb	(mdd)	5.2	1.5	1.6	1.6	14.0	4.9	7.4	2.4	6.8	10.4	10.6
Pr	(mdd)	11.9	4.4	4.4	8.4	33.9	11.6	16.3	1.7	15.7	7.0	8.9
Nd	(mdd)	43.5	18.6	18.1	37.0	105	46.2	64.2	7.3	64.2	29.2	28.3
Sr	(mdd)	944	385	375	443	305	503	296	68	286	346	337
Zr	(mdd)	259	139	139	250	1027	225	282	77	247	184	187
Hf	(mdd)	5.7	3.5	3.5	6.3	23.7	5.6	7.0	1.9	6.2	5.0	5.0
Sm	(mdd)	8.2	4.7	4.5	9.3	14.4	9.4	13.3	1.9	12.7	6.9	6.5
Eu	(mdd)	2.6	1.6	1.5	3.0	3.9	3.0	4.1	9.0	3.8	2.1	2.0
Gd	(mdd)	8.9	4.7	4.7	0.6	10.2	8.2	11.2	2.0	11.3	7.1	6.8
Tb	(mdd)	1.0	0.8	0.8	1.4	1.6	1.2	1.5	0.3	1.5	1.2	1.1
Dy	(mdd)	5.4	4.6	4.6	7.9	8.9	6.1	7.8	1.8	8.0	7.0	6.4
Но	(mdd)	1.0	6.0	6.0	1.5	1.6	1.0	1.4	0.4	1.5	1.5	1.3
X	(mdd)	24.5	21.9	21.4	36.0	37.3	24.6	39.0	9.5	57.1	36.2	36.1
Er	(mdd)	2.3	2.2	2.2	3.7	4.1	2.2	3.1	1.0	3.8	3.8	3.7
Tm	(mdd)	0.3	0.3	0.3	0.5	9.0	0.3	0.4	0.1	0.5	0.5	0.5
Yb	(mdd)	1.8	1.8	1.8	2.7	3.4	1.5	2.1	0.8	2.7	3.3	3.4
Lu	(mdd)	0.2	0.3	0.3	0.4	0.5	0.2	0.3	0.1	0.4	0.5	0.5
Sc	(mdd)	22.2	25.7	24.8	33.0	0.1	23.9	27.0	18.4	24.6	33.4	33.5
,												

¹Major elements and select trace elements for whole rock samples were measured by XRP at WSU. These samples were analyzed together with USGS reference material BCR-2, and the BCR-2, and the BCR-2, and the ALIA-121-09. reference values from Jochum et al. (2016) are provided in the table. Major element data are not available for samples RR1310-D40-10, RR1310-D34-01, KK8203-DR-4, KK8203-DR-5, RR1310-D29-01, and ALIA-121-09.

²Trace elements for whole rock powders were analyzed by solution ICP-MS at WSU. The reference material BCR-2 was analyzed as an unknown with these samples. The new BCR-2 data are shown with the preferred values from Jochum et al. (2016). Trace element data are not available for samples RR1310-D34-01, and RR1310-D40-10.

³Two different totals are included for major element analyses. The first total includes major element oxide analyses, loss on ignition (LOI), and the trace element totals expressed as oxides and includes the following trace elements: Ni, Cr, Sc, V, Ba, Rb, Sr, Zr, Y, Nb, Ga, Cu, Zn, Pb, La, Ce, Th, Nd, and U.

Downloaded from https://academic.oup.com/petrology/article/63/5/egac032/6563380 by University of California, Santa Barbara user on 05 June 2022

Table 4. Major and trace element analyses of glasses examined in this study

Sample name	PPT-D1-N1	PPT-D1-N1 2RSD (%)	PPT-D1-N2	PPT-D1-N2 2RSD (%)	ALV 519-4-1	ALV 519-4-1 2RSD (%)	Preferred ALV 519-4-1 (Melson et al., 2002; Gale
		•		,			et al., 2013a, 2013b)
Volcano	Papatua	Ι	Papatua	Ι			
Material analyzed	Glass	I	Glass	-	Glass	-	
Method of major element analysis	sis EPMA 1 - AVG of 3	1	EPMA 1 - AVG of 3	-	$EPMA^1$ - AVG of 22	1	1
Method of trace element analysis	is LA-ICP 2 - AVG of 2		LA-ICP 2 - AVG of 3	_	$LA-ICP^2$ - AVG of 8	1	-
EPMA majors							
•	42.44	1.6	42.81	1.1	48.98	1.5	48.94
	4.12	0.4	4.11	1.3	0.73	1.3	0.77
Al_2O_3 (wt %)	13.18	2.5	13.27	1.2	16.44	1.8	16.53
	11.69	2.0	11.83	0.3	8.91	0.8	9.03
	0.19	4.4	0.19	2.3	0.17	5.2	1
	98.9	0.8	6.55	3.2	9.71	2.0	9.41
	13.14	1.5	13.22	2.1	12.48	9.0	12.58
Na_2O (wt %)	3.56	0.7	3.47	4.3	2.10	2.5	2.07
K_2O (wt %)	1.71	2.9	1.68	0.7	0.08	4.5	0.10
P_2O_5 (wt %)	1.21	1.7	1.18	0.5	0.07	19.0	60.0
	09'.26	I	98.31	I	99.66	I	99.52
LA-ICP traces (PPT glasses, ALV 519-4-1)	519-4-1)						
Ni (mdd)		14.9	58.6	4.2	188.8	2.6	178.0
Cu (mdd)	68.3	17.3	63.9	6.5	107.8	2.2	98.0
	163.8	2.1	164.4	4.1	82.9	5.5	I
Li (ppm)	11.6	6.1	11.3	2.6	4.2	2.7	4.2
	42.9	2.6	44.5	1.8	51.2	1.5	48.7
	0.5	2.6	0.5	5.0	0.0	44.1	0:0
	41.0	3.0	41.1	5.1	2.1	2.2	2.0
	633.6	2.1	615.8	1.2	24.4	2.1	24.3
	10.2	4.2	10.0	0.2	0.3	4.7	0.3
	2.6	0.5	2.5	6.0	0.1	6.9	0.1
	88.1	0.5	86.3	2.8	4.0	1.2	4.5
	4.6	3.5	4.6	2.1	0.2	7.3	0.3
La (ppm)	97.6	9.0	95.0	3.2	2.7	2.2	2.8
	207.3	0.7	200.0	3.9	8.9	1.4	6.9
	9.3	5.3	8.9	3.8	0.2	6.6	0.3
	21.6	1.2	21.4	9.0	6.0	1.9	1.0
							(Continued)

Downloaded from https://academic.oup.com/petrology/article/63/5/egac032/6563380 by University of California, Santa Barbara user on 05 June 2022

Table 4. Continued

κχ	Sample name	PPT-D1-N1	PPT-D1-N1 2RSD (%)	PPT-D1-N2	PPT-D1-N2 2RSD (%)	ALV 519-4-1	ALV 519-4-1 2RSD (%)	Preferred ALV 519-4-1 (Melson et al., 2002; Gale et al., 2013a, 2013b)
Nd	(mdd)	86.8	6.0	86.5	1.5	4.9	3.3	5.2
Sr	(mdd)	1180.0	4.3	1150.0	1.1	64.3	1.2	71.0
Zr	(mdd)	417.5	3.6	418.3	5.4	34.5	1.2	39.9
Hf	(mdd)	8.2	2.3	8.4	6.0	6:0	3.4	1.1
Sm	(mdd)	15.5	1.8	15.5	2.0	1.6	6.1	1.7
Eu	(mdd)	4.4	2.1	4.3	1.9	9.0	3.3	0.7
Gd	(mdd)	12.1	1.4	12.2	3.0	2.3	4.5	2.6
Tb	(mdd)	1.5	1.7	1.5	4.0	0.4	4.9	0.5
Dy	(mdd)	8.8	3.3	8.8	2.5	3.2	1.6	3.4
Но	(mdd)	1.5	1.2	1.5	5.4	0.7	3.7	0.8
Y	(mdd)	38.5	1.8	38.9	2.7	18.6	1.7	22.3
Er	(mdd)	3.8	6.7	3.8	2.9	2.2	3.4	2.3
Tm	(mdd)	0.5	3.2	0.5	5.5	0.3	5.4	
Yb	(mdd)	2.9	5.1	2.9	4.7	2.3	4.5	2.4
Lu	(mdd)	0.4	0.7	0.4	1.5	0.3	3.8	0.4
Sc	(mdd)	27.8	4.1	28.5	3.3	42.6	1.3	43.0

¹Major elements on Papatua (PPT) glasses were measured by electron probe microanalyzer (EPMA) at UCSB. The standard reference material ALV 519-4-1 was run together with the PPT glasses in the analyzer in the EPMA data consist of an average of several analyses of the same sample (the number of analyses is noted at the top the data table), and the 2RSD reproducibility for multiple EPMA analyses is also provided. These data are provided with preferred values from Melson et al. (2002).

Trace elements for the PPT glasses were measured by laser ablation inductively coupled plasma mass spectrometer (LA-ICP-MS) at Clermont-Ferrand along with the reference material ALV 519-4-1. These data are provided with preferred values from Melson et al. (2013a, 2013b). Note that the LA-ICP-MS data consist of an average of several analyses of the same sample (the number of analyses is noted at the top the data table), and the ZRSD reproducibility for multiple LA-ICP-MS analyses is also provided.

Downloaded from https://academic.oup.com/petrology/article/63/5/egac032/6563380 by University of California, Santa Barbara user on 05 June 2022

Table 5. Hf-Pb-Sr-Nd isotopic data for samples analyzed in this study¹

Sample name	Location	176Hf/ 177Hf	2SE	Hf isotopes measured	²⁰⁶ Pb/ ²⁰⁴ Pb	2SE	²⁰⁷ Pb/ 2	2SE 208	²⁰⁸ Pb/ 2SE ²⁰⁴ Pb	. Pb isotopes measured	s ⁸⁷ Sr/	2SE 8	Sr isotopes measured	¹⁴³ Nd/ ¹⁴⁴ Nd	2SE N	Nd isotopes measured
				at	1		1			at			at			at
PPT-D1-N1 glass PPT-D1-N2 glass	Papatua Papatua	0.282892	0.000000	Lyon	18.6861	0.00037	15.6324 0.0 15.6284 0.0	0.0030 38.8	38.8835 0.0063 38.9221 0.0008	53 Lyon 38 Lyon	0.705045	0.000008	- NC	0.512631 0.00	0.000007	UNC
RR1310-D41-05	Lalla	0.283048	0.000003	Lyon	19.4521	0.0004			39.8335 0.0009		0.705000	0.000008	UNC		0.000011	UNC
RR1310-D40-10 clast	Kookn Lalla	0.282960	0.000075	Lyon	19.1582	0.0059 15.6487		0.0043 39.6	39.6997 0.0131	31 Lyon	0.704970	0.000010	UNC	0.512750 0.000004	20004	UNC
RR1310-D39-01	Rookh Siafiafi	0.282977	0.000005	Lyon	19.4640	0.0006	15.6195 0.0	0.0005 39.7	39.7449 0.0015	l5 Lyon	0.705030	0.000008	UNC	0.512792 0.00	0.00000	UNC
ALIA-D121-09 clast	Siafiafi	I		,	19.7439	0.0012	15.6305 0.0	0.0011 40.0	40.0489 0.0023		I	I		0.512775 0.00	0.000005	UNC
ALIA-D121-09 clast rep	Siafiafi	I			I		I			. 1	0.704519	0.00000.0	UCSB		1	
RR1310-D29-10	Bustard	0.283040	0.000006	Lyon	18.7645	0.0004 1	15.5792 0.0	0.0003 38.7	38.7311 0.0008	38 Lyon	0.704102	0.000010	UNC	0.512838 0.00	0.000005	UNC
RR1310-D34-01	Tuscarora	Tuscarora 0.282872	0.000004	Lyon	18.7671	0.0018 1	15.6655 0.0	0.0015 38.8	38.8700 0.0037	37 Lyon	0.707822	0.000008	UNC	0.512539 0.00	0.000005	UNC
KK8203-DR-9 clast	Tuscarora 0.283112	0.283112	0.000004	Lyon	18.9237		15.5627 0.0	0.0003 38.7	38.7687 0.0008	18 Lyon	0.703789	0.000011	UNC	0.512921 0.00	0.000004	UNC
RR1310-D38-08	Waterwitch 0.283056	า 0.283056	0.000004	Lyon	19.6015	0.0004 1	15.5979 0.0	0.0004 39.5	39.5445 0.0009	19 Lyon	0.703727	0.000008	UNC	0.512890 0.00	0.000004	UNC
RR1310-D38-08 rep 1	Waterwitch		I		I	I	I	ı	1		0.703720	0.000005	UCSB	0.512897 0.00	0.000002	UCSB
RR1310-D38-08 rep 2	Waterwitch					I	1		1		0.703725	9000000.0	UCSB			
KK8203-DR-1 clast	Talviuni	0.283035	0.000005	Lyon	19.0401	0.0011 1	15.5932 0.0	0.0007 39.4	39.4478 0.0028	28 Lyon	0.704271	0.000008	UNC	0.512857 0.00	0.000004	UNC
RR1310-D31-01	Fa'aitu	I					1	1	1		0.704633	0.000005	UCSB	0.512765 0.00	0.000002	UCSB
RR1310-D31-01 rep	Fa'aitu	I			18.7733	0.0031	15.5826 0.0	0.0025 38.8	38.8583 0.0066	96 USC	0.704642	0.000007	UCSB			
RR1310-D31-02	Fa'aitu	Ι	I	I	I	I	I	· 	1	I	0.704586	900000000	UCSB	0.512771 0.000002	20000	UCSB
RR1310-D31-02 rep	Fa'aitu	1		l	18.7650	0.0003 1	15.5736 0.0	0.0003 38.8	38.8240 0.0011	11 USC	0.704588	90000000	UCSB	0.512765 0.00	0.000003	UCSB
USGS reference materials:																
BCR-2, UCSB/USC		I			18.7543	0.0004 1	15.6188 0.0	0.0004 38.7	38.7162 0.0013	13 NSC	0.705003	9000000.0	UCSB	0.512620 0.000002	20002	UCSB
BCR-2, UCSB/USC		I		1		I	I		1		0.705007	9000000:0	UCSB	0.512621 0.00	0.000002	UCSB
BCR-2, UCSB/USC		I	I	I	18.7415	0.0004 1	15.6093 0.0	0.0004 38.6	38.6795 0.0013	.3 USC	0.705006	9000000:0	UCSB	0.512625 0.00	0.000003	UCSB
BCR-2, Lyon/UNC		0.282886	0.000005	Lyon	18.7588	0.0009	15.6251 0.0	0.0008 38.7	38.7414 0.0022	2 Lyon	0.704989	0.000010	UNC	0.512625 0.00	0.000005	UNC
BCR-2, Weis et al. (2006,	I	0.282870	0.000008	1	18.7533	0.0195 1	15.6262 0.0	0.0040 38.7	38.7282 0.0405		0.705005	0.000010	I	0.512622 0.00	0.000012	1
2007)																
BCR-2, avg. Woodhead				l	18.7543	0.0110	15.6217 0.0	0.0030 38.7	38.7186 0.0210	- 0:			I	I	I	l
AGV-2, Lyon/UNC	I	0.282989	0.000004	Lyon	18.8660	0.0009	15.6174 0.0	0.0009 38.5	38.5299 0.0032	32 Lyon	0.703995	0.000008	UNC	0.512769 0.00	0.000005	UNC
AGV-2, Weis et al. (2006,	1	0.282984	0.00000		18.8692	0.0063 1	15.6186 0.0	0.0071 38.5	38.5488 0.0135		0.703973	0.000005	I	0.512774 0.00	0.000010	I
2007)																

Jolla to JNdi conversion from Tanaka et al. (2000) was used for ¹⁴³Nd/¹⁴⁴Nd). A BCR-2 and an AGV-2 (both labeled "Lyon/UNC") were reported previously (Jackson et al., 2017; Price et al., 2017), but were analyzed together with samples reported here, so are provided in the table for completeness (but are renormalized to preferred standard values used here). Errors for sample unknowns are 2\sigma standard error of the mean (and represent are absolute (not relative). Errors on the USGS reference materials from Weis et al. (2006) represent 2 SD and represent multiple analyses of a USGS reference material. Measurements in this study were made (or repeated) at several institutions. We indicate when measurements were made at Lyon, USC, UNC, or UCSB. within error to the preferred value of 0.282163±0.000009 (Blichert-Toft et al., 1997); hence, no corrections were applied to the new 176Hf1/17H data. Isotopic compositions for all other data in the table (including previously published geologic reference materials) are normalized to an NBS987 value of 0.710240 for 87 Sr/86Sr, a INdi 143 Nd/144 Nd value of 0.512099 (INdi value from Garçon et al., 2018), and Pb isotopic compositions or NBS981 from Eisele et al. (2003) (i.e., 206 pb/2⁰⁴ pb = 16.9409, ²⁰⁷ pb/²⁰⁴ pb = 15.4976, and ²⁰⁸ pb/²⁰⁴ pb = 36.7262). Data for USGS reference materials are renormalized to preferred standard values used here (and a La With the exception of two Papatua glasses, isotopes were measured on rock chips (not powders). The unweighted mean 176Hf/177Hf of the JMC-475 Hf standard run alternately with the samples were identical

JNdi $(0.512103 \pm 0.000012, 2 SD, N = 7)$ and preferred JNdi (0.512099; Garçon et al., 2018).

The samples processed for wet chemistry and mass spectrometry at ENS Lyon and UNC were run together with the same suite of unleached USGS reference materials (BCR-2 and AGV-2) as the basalt samples published in Jackson et al. (2017) and the isotopic compositions are listed in Table 5 for completeness. The total procedural Pb and Hf blanks for the samples processed at ENS Lyon are both <20 pg, while the Sr and Nd blanks for the samples processed at UNC are <100 pg and < 50 pg, respectively.

Analyses carried out at UCSB and USC

A subset of samples reported here were analyzed (or re-analyzed) at UCSB and USC. The same heavy leach method used at ENS Lyon (described above) was applied to all samples run at UCSB, except RR1310-D31-01 and RR1310-D3102, which were subjected to only the light leach method because they were extremely fresh. Following sample digestion, Sr and Pb separations were carried out at UCSB by two passes through $100-\mu l$ Eichrom Sr-spec columns (based on Konter & Storm, 2014). Sample loading and mass spectrometry followed methods described in Jackson et al. (2020) and are summarized here. Approximately 500 ng Sr was loaded on outgassed, zone-refined (99.999% purity, H-Cross, USA) Re filaments with TaCl emitter. Analyses were carried out on a Thermo Scientific Triton Plus TIMS housed at UCSB, employing amplifier rotation on 10¹¹ ohm amplifiers and a 3.3 picoamp gainboard; 2 h gains were run every other day (with the start of a new barrel). Each analysis lasted for 1 h (excluding interblock heating and focusing), and ~20% of analysis time was devoted to baseline measurements (made with each rotation of the amplifiers). During analysis, the beam was kept at or near 3 V on mass 88. Long-term reproducibility of NBS987 analyses on the UCSB Triton Plus—which had been operating at UCSB for ~3 months at the time of the new analyses reported here—was 0.710246 ± 0.000011 (N = 29, 2 SD). The measured Sr isotopic compositions were corrected for instrumental mass fractionation as indicated above. Sample unknowns and the USGS reference material (BCR-2) were corrected for the offset between preferred (0.710240) and measured ⁸⁷Sr/⁸⁶Sr of NBS987 analyzed in the same barrel.

Neodymium was purified by passing the Sr column washes through a series of columns filled with TRUand Ln-spec resins (following Price et al., 2014). Sample loading and mass spectrometry followed the methods in Jackson et al. (2020) and is summarized here. Approximately 500 ng Nd aliquots were loaded on outgassed, zone-refined (99.999% purity, H-Cross, USA) Re filaments and analyzed for ¹⁴³Nd/¹⁴⁴Nd on the UCSB Triton Plus TIMS. Analyses employed amplifier rotation on the same amplifiers and gain board as described above; 2 h gains were run every other day (with the start of a new barrel). Analyses lasted for 2 h, and baselines were run for \sim 20%

of each analysis (with each rotation of the amplifiers). Signal intensities were kept at or near 3 V on mass 142. The long-term average reproducibility (up to and including this study) of 143Nd/144Nd on JNdi analyses on the UCSB Triton Plus was 0.512100 ± 0.000004 (2 SD, N = 27). Instrumental mass fractionation correction assumed an exponential fractionation law and a 146Nd/144Nd ratio of 0.7219. Sample unknowns and the BCR-2 reference material were corrected for the offset between preferred (0.512099) and measured 143 Nd/ 144 Nd on JNdi analyzed in the same barrel.

Lead isotopic compositions were measured at USC on a Thermo-Neptune MC-ICP-MS following the protocols described in Béguelin et al. (2017) and Jackson et al. (2020). Samples were corrected for instrumental fractionation using Tl addition (see White et al., 2000 for details) and assuming an exponential fractionation law. The samples, along with unleached aliquots of BCR-2 processed with the sample unknowns, were corrected for the offset between preferred (from Eisele et al., 2003) and measured ratios of NBS981. The total procedural blanks for Sr, Nd, and Pb for the samples processed at UCSB and USC are <200 pg, <50 pg, and <120 pg, respectively.

RESULTS

40 Ar/39 Ar age data

Plagioclase separates from three samples (i.e., RR1310-D31-01 and RR1310-D31-02 from Fa'aitu and RR1310-D38-08 from Waterwitch) and two groundmass samples (RR1310-D38-41 from Waterwitch and RR1310-D29-01 from Bustard) were targeted for ⁴⁰Ar/³⁹Ar dating (Fig. 3). All three plagioclase separates produced sufficiently long plateaus (67–100% ³⁹ Ar released), probability of fit values >5%, and ⁴⁰Ar/³⁶Ar intercept values within error of the atmospheric ratio $(^{40}Ar/^{36}Ar = 295.5)$ used for standard corrections at time of analyses) (Table 2) to support a robust designation for the ages. The Waterwitch plagioclase separate from sample RR1310-D38-08 provided a weighted-plateau age of 10.49 ± 0.09 (2 σ) Ma (Figs 1 and 3). Although the groundmass incremental heating results for Waterwitch sample RR1310-D38-41 provided a discordant age spectrum (indicative of significant recoil effects) and was interpreted to not provide an eruption age, the intermediate temperature steps are close to the 10.4–10.6 Ma plagioclase age range from sample RR1310-D38-08 from the same dredge haul. The two Fa'aitu plagioclase separates yielded younger ages of 1.26 ± 0.14 Ma and 1.48 ± 0.19 Ma (Table 2). The Bustard groundmass yielded a mini-plateau (41% ³⁹Ar released; 7 consecutive steps) age of 3.47 ± 0.02 Ma (Table 2, Fig. 3). We choose to include this age in our discussion as the heating spectrum plateau length was reduced at either end by short bursts of excess ⁴⁰Ar (data points falling well outside the best fit inverse isochron line and pointing toward the origin), which produced anomalously old apparent ages. We recommend this sample age be treated with caution given the narrow plateau.

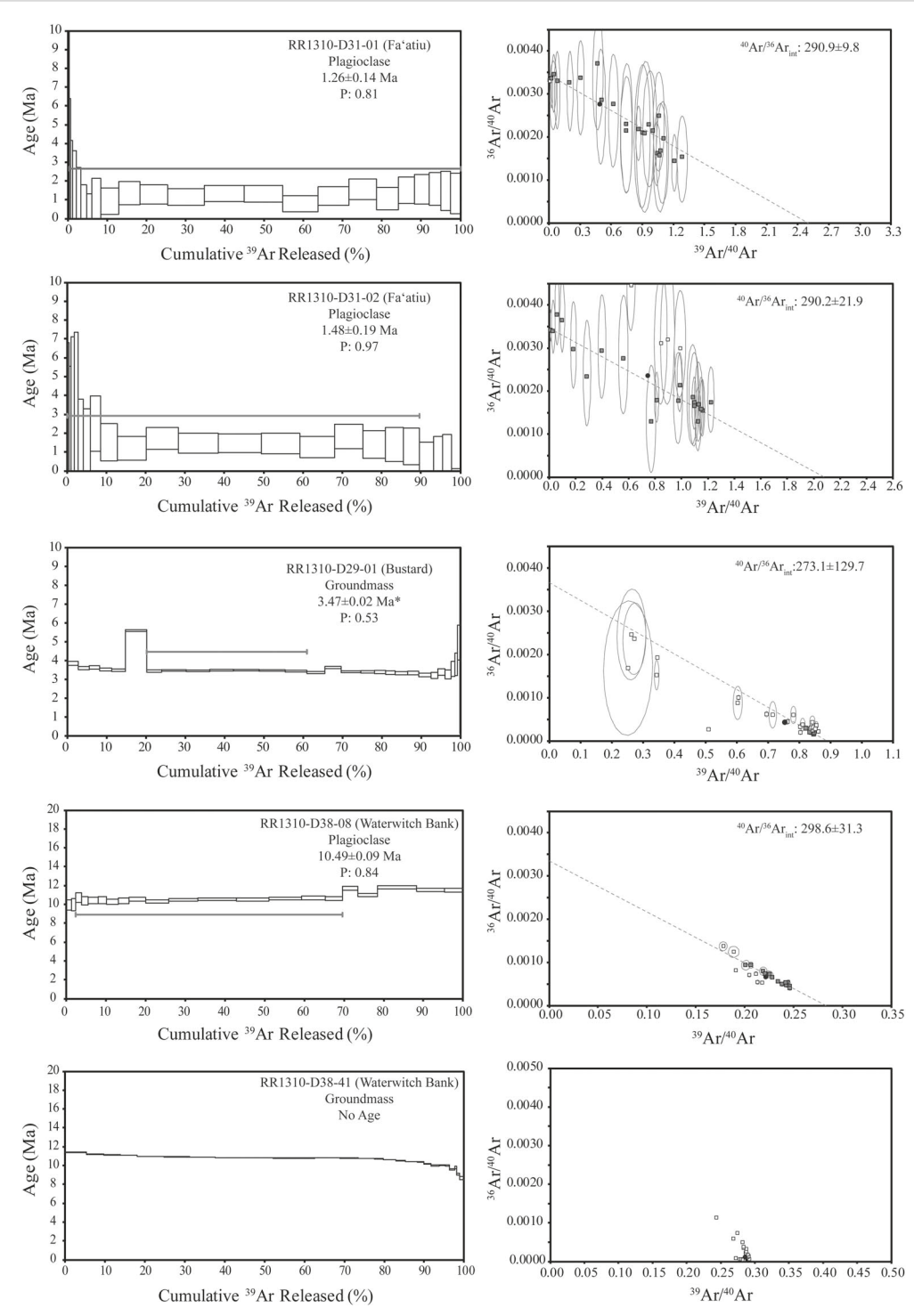


Fig. 3. 40 Ar/39 Ar age determination results. Incremental heating (left) and inverse isochron (right) 40 Ar/39 Ar analyses for Fa'aitu, Bustard, and Waterwitch seamounts. The portion of the plateaus used in the age calculations are indicated with gray lines. Filled squares in the inverse isochrons represent steps used in the plateau age calculation. Dashed lines represent the best fit isochrons with the corresponding initial 40 Ar/36 Ar values shown. Uncertainties are shown with 2σ confidence. Data are listed in Table 2.

Major element compositions

The lavas in this study cover a wide range of compositions (Tables 3 and 4, Supplementary Figure S1); however, all but two samples (RR1310-D31-01 and RR1310-D31-02) are alkalic. The two Fa'aitu samples, RR1310-D31-01 and RR1310-D31-02, are transitional in total alkalis versus SiO₂ (MacDonald & Katsura, 1964). The two Papatua glasses (PPT-D1-N1 and PPT-D1-N2) and the Bustard lava (RR1310-D29-10) fall in the tephritebasanite field, while the samples from Lalla Rookh seamount (RR1310-D41-05) and Waterwitch seamount (RR1310-D38-08) fall in the alkali basalt field. The most evolved lava in this study, RR1310-D39-01 from Siafiafi seamount, with MgO of 0.92 wt %, is a phonolite.

Samples RR1310-D40-10, RR1310-D34-01, KK8203-DR-1, KK8203-DR-9, RR1310-D29-01, and ALIA-121-09 were not analyzed for major elements, due to too little sample material being available; hence, a compositional designation for the rock type cannot be made.

Trace element compositions

The lavas in this study exhibit a wide variety of trace element abundances (Tables 3 and 4), which are displayed in primitive mantle-normalized (McDonough & Sun, 1995) trace element diagrams (Supplementary Figure S2). The two Papatua glasses (PPT-D1-N1 and PPT-D1-N2) are strongly enriched in incompatible trace elements and show negative K, Pb, Zr, Hf, and Ti anomalies. Sample RR1310-D41-05 from Lalla Rookh shows strong incompatible trace element enrichment and has slight negative Cs, Ba, U, K, and Pb anomalies. Due to limited sample size, basalt clasts separated from a hyaloclastite from Lalla Rookh sample RR1310-D40-10 were not analyzed for trace elements. The primitive mantle-normalized trace element pattern displayed by the newly analyzed Waterwitch sample (RR1310-D38-08) has strong negative K and Pb anomalies. The two samples from Fa'aitu (RR1310-D31-01 and RR1310-D31-02) exhibit nearly identical primitive mantle-normalized trace element patterns and are moderately enriched in incompatible trace elements, except for strong depletions in Cs and Pb and a positive Sr anomaly. Two samples from Siafiafi, RR1310-D39-01 and the basalt clast separated from hyaloclastite sample ALIA-D121-09, have dissimilar primitive mantle-normalized trace element patterns: sample RR1310-D39-01 has higher incompatible trace element concentrations than the ALIA-D121-09 clast, consistent with its highly differentiated phonolite composition, which also explains its 'spikier' pattern, with strong depletions in Ba, U, Pb, Sr, and Ti. Sample KK8203-DR-1, a basalt clast separated from a Talviuni seamount sample, has a primitive mantle-normalized trace element pattern that is broadly similar to Siafiafi sample ALIA-D121-09. Tuscarora bank sample KK8203-DR-9—the most geochemically depleted sample in this study—shows slight enrichment in several incompatible trace elements, including positive Pb, Zr, and Hf anomalies, as well as negative Ba and Sr anomalies. The Bustard seamount sample (RR1310-D29-10) shows strong incompatible trace element enrichment and a positive Sr anomaly (unfortunately, due to its small sample size, trace element data are not available for a second Tuscarora seamount sample RR1310-D34-01).

Hafnium, Pb, Sr, and Nd isotopic compositions

Based on their varied geochemical compositions, we group the lavas from this study into three categories-EM1-type lavas, geochemically enriched WESAM lavas, and WESAM lavas with depleted isotopic compositions and we explore each category in detail below.

EM1-type lavas

The samples from Papatua seamount and Fa'aitu seamount studied here show EM1-like isotopic characteristics (Fig. 4). The glasses from Papatua seamount, PPT-D1-N1 and PPT-D1-N2, have 143Nd/144Nd ranging from 0.512622 to 0.512631, ⁸⁷Sr/⁸⁶Sr of 0.705045, ¹⁷⁶Hf/¹⁷⁷Hf ranging from 0.282877 to 0.282892, and ²⁰⁶Pb/²⁰⁴Pb ranging from 18.6861 to 18.7229. The two samples from the WESAM Fa'aitu seamount, RR1310-D31-01 and RR1310-D31-02, have nearly identical isotopic compositions with weak EM1-like signatures. They have 143Nd/144Nd ranging from 0.512765 to 0.512771, 87 Sr/86 Sr ranging from 0.704586 to 0.704642, and ²⁰⁶Pb/²⁰⁴Pb ranging from 18.7650 and 18.7733.

Western Samoan (WESAM) lavas with geochemically enriched isotopic compositions

We report data from seven samples with moderately enriched geochemical compositions. Two lavas from Lalla Rookh seamount (sample RR1310-41-05 and the basaltic clasts taken from hyaloclastite sample RR1310-40-10) have isotopic signatures comparable to lavas previously dredged from Lalla Rookh seamount (Hart et al., 2004), but have slightly higher 87Sr/86Sr (up to 0.705000) and ¹⁴³Nd/¹⁴⁴Nd as low as 0.512750 (Fig. 4). Siafiafi seamount lava RR1310-D39-01 shows isotopic similarities to the Lalla Rookh samples from this study and Hart et al. (2004), while the basalt clast from Siafiafi hyaloclastite sample ALIA-D121-09 has slightly more radiogenic Pb (206Pb/204Pb of 19.7439). Additionally, basaltic clast sample ALIA-D121-09 has slightly lower 87Sr/86Sr (0.704519) than the Siafiafi seamount lava (0.705030), but similar $^{143}Nd/^{144}Nd$ (0.512775). The ⁸⁷Sr/⁸⁶Sr from the Siafiafi ALIA-D121-09 basaltic clast has similar ⁸⁷Sr/⁸⁶Sr (0.704519) to the previously published ⁸⁷Sr/⁸⁶Sr of a clinopyroxene megacryst separated from the same hyaloclastite sample (0.704587; see sample ALIA-D121-09 in Jackson et al., 2010). A basalt clast from Talviuni hyaloclastite sample KK8203-DR-1 has lower 206 Pb/ 204 Pb (19.0401) and 87 Sr/ 86 Sr (0.70427) than the Lalla Rookh sample RR1310-D40-10 clast, but higher 176 Hf/ 177 Hf (0.283035) and 143 Nd/ 144 Nd (0.512857). One Tuscarora bank lava, RR1310-D34-01, has even more enriched isotopic signatures than the five lavas discussed above, with ⁸⁷Sr/⁸⁶Sr of 0.707822, ¹⁴³Nd/¹⁴⁴Nd of 0.512539, 176 Hf/ 177 Hf of 0.282872, and 206 Pb/ 204 Pb of 18.7671. The Waterwitch seamount lava RR1310-D38-08 has one of the most radiogenic Pb isotopic compositions in this study (206 Pb/204 Pb of 19.6015) (Fig. 4). This Waterwitch sample has slightly lower 143 Nd/144 Nd (0.512890) than the previous Waterwitch sample from Jackson et al. (2010), but has similar ⁸⁷Sr/⁸⁶Sr (0.703727) and more radiogenic Pb isotopic compositions.

Western Samoan (WESAM) lavas with geochemically depleted isotopic compositions

We also report isotopic data for a Bustard seamount lava (RR1310-D29-10) and a combination of basaltic

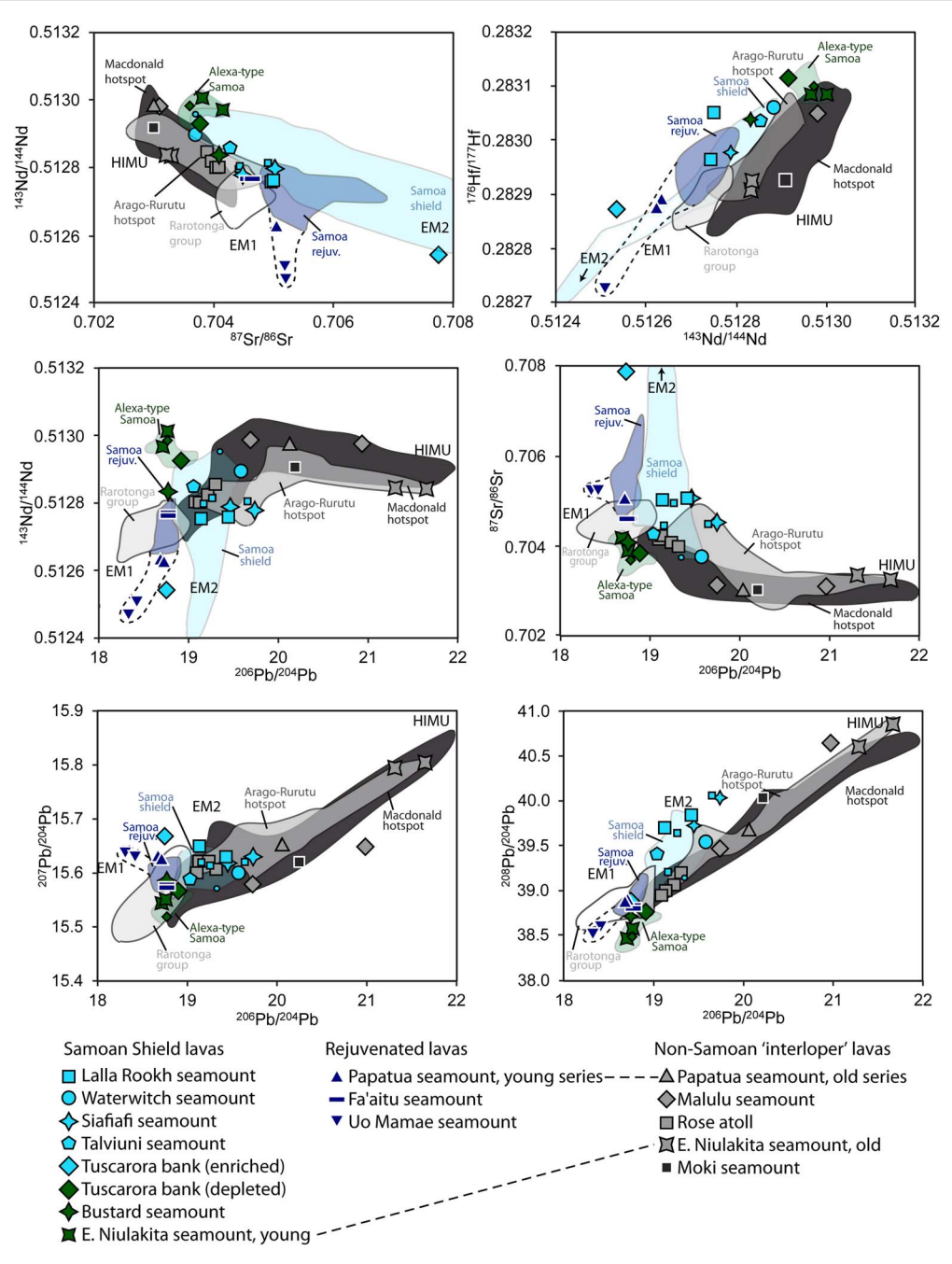


Fig. 4. Strontium, Nd, Hf, and Pb isotopic variations for lavas in this study. The data are divided into the following fields: Samoan shield, Samoan rejuvenated, Alexa-type Samoa (geochemically depleted Samoan shield), Arago-Rurutu hotspot, Rarotonga group, and Macdonald hotspot. For the following seamounts, previously published data are distinguished from data of this study by smaller symbol size, and include data from Waterwitch seamount (Jackson et al., 2010), Lalla Rookh seamount (Hart et al., 2004), and Tuscarora seamount (Finlayson et al., 2018). Additionally, previously published data on lavas from the older series of Papatua (Jackson et al., 2010), Uo Mamae (Pearce et al., 2007; Regelous et al., 2008), Malulu seamount, Rose atoll, Moki seamount (Jackson et al., 2010; Buff et al., 2021), as well as older Arago-Rurutu hotspot-sourced and younger Samoa hotspot-sourced lavas from East Niulakita (Finlayson et al., 2018) are also shown with separate symbols. A dashed line extends to connect the Samoan rejuvenated field to Uo Mamae (which is likely genetically related to Samoan rejuvenated lavas; Regelous et al., 2008) and encompasses the Papatua seamount glasses. The Samoa shield field comprises data for ESAM shield lavas, while the Samoa rejuvenated field comprises data for ESAM rejuvenated lavas and lavas from Wallis Island. Data forming the Samoan fields are from the following studies: Wright & White (1987), Workman et al. (2004), Workman & Hart (2005), Jackson et al. (2007a, 2007b, 2010), Salters et al. (2011), Price et al. (2014), and Finlayson et al. (2018). The Macdonald, Arago-Rurutu (the <10 Ma Cook-Austral data), and Rarotonga data fields are from Jackson et al. (2020), and the Arago-Rurutu field has been expanded to include the old volcanic stage of East Niulakita.

clasts from a Tuscarora bank hyaloclastite (KK8203-DR-9), which exhibit relatively depleted geochemical compositions. The basaltic clasts from Tuscarora bank sample KK8203-DR-9 has much lower ⁸⁷Sr/⁸⁶Sr (0.703789) than the other Tuscarora bank lava in this study (see sample RR1310-D34-01 [with 87Sr/86Sr = 0.707822] above) (Fig. 4). Notably, the Tuscarora KK8203-DR-9 clasts show similar 87 Sr/ 86 Sr, 143 Nd/ 144 Nd, and 176 Hf/ 177 Hf but slightly more radiogenic Pb isotopes than the only other Tuscarora bank sample (RR1310-D33-32; Finlayson et al., 2018), which was dredged during a different expedition (Fig. 4). Bustard seamount has similar Pb isotopic compositions to Tuscarora bank sample KK8203-DR-9, but also has slightly higher ⁸⁷Sr/⁸⁶Sr (0.704102), lower ¹⁴³Nd/¹⁴⁴Nd (0.512838) and lower 176 Hf/ 177 Hf (0.283040).

DISCUSSION

Given that Samoan lavas exhibit such a wide variety of isotopic compositions, we explore changes in isotopic composition of lavas along the Samoan chain (Fig. 5). The lavas with the most geochemically depleted ⁸⁷Sr/⁸⁶Sr (i.e. Alexa-type lavas) and lowest 206Pb/204Pb appear in the western region of the Samoan hotspot track, and the lavas with the most geochemically enriched ⁸⁷Sr/⁸⁶Sr and highest ²⁰⁶Pb/²⁰⁴Pb tend to be located in the eastern region of the hotspot track.

Tracing the "hotspot highway"

The "hotspot highway" consists of multiple overlapping hotspot tracks aligned on a Pacific plate flow line, where the result of the overlapping hotspot tracks is a linear suite of islands and seamounts that show no clear volcanic progression unless the volcanoes are separated by their respective hotspots of origin (see Fig. 1b and 1c). In addition to the Samoan hotspot track, the hotspot highway includes the Cook-Austral Volcanic Lineament, suggested by Chauvel et al. (1997) to consist of three individual age-progressive hotspot tracks: the Macdonald hotspot (also referred to in the literature as the "Tubuai trend" and "Old Rurutu"), the Arago-Rurutu hotspot (referred to as the "Atiu trend" and "Young Rurutu"), and the Rarotonga group. This is relevant because the hotspot highway hypothesis predicts that older volcanoes associated with these three hotspots are located in the Samoan region (Jackson et al., 2010). This hypothesis successfully explains, for example, the presence of the Arago-Rurutu hotspot-related volcano Rose atoll (Figs 1 and 2) near the eastern terminus of the Samoan hotspot track and likely explains the presence of two undated HIMU volcanic interlopers—Malulu seamount and the HIMU stage of Papatua seamount in the region near the Samoan hotspot (Buff et al., 2021). In the following, we explore the western (older) extents of the hotspot tracks that constitute the hotspot highway and attempt to deconvolve contributions of these hotspots to the hotspot highway with particular emphasis on determining the origin of the older HIMU stage of volcanism at Papatua.

Macdonald hotspot

Based on the Wessel & Kroenke (2008) plate motion model, the trace of the Macdonald hotspot track continues from Macdonald seamount to the Samoan region, where the hotspot trace bends north at ~50 Ma,

a bend that is similar morphologically to the Hawaii-Emperor Bend (HEB) in the region near the Samoan hotspot (Fig. 1). Therefore, volcanic contributions from the Macdonald hotspot are expected (1) in the region between the Samoan hotspot and Macdonald seamount; and (2) along a trace extending to the NNW of the Samoan region into the Tokelau Islands where the Macdonald hotspot can be traced back to \sim 70 Ma (Koppers et al., 2007; Konter et al., 2008; Jackson et al., 2020). Critically, the plate reconstruction predicts that volcanoes related to Macdonald hotspot would not be found to the west of the main Samoan islands of the ESAM region (Figs 1 and 2). Within uncertainty of the Wessel & Kroenke (2008) plate reconstruction model, two Samoan interloper seamounts—Malulu seamount and the HIMU stage of Papatua seamount—may have been generated over the Macdonald hotspot, in which case they would have predicted ages of \sim 43 to \sim 44 Ma. Unfortunately, samples suitable for dating have not yet been obtained from these two seamounts.

Arago-Rurutu hotspot

The Wessel & Kroenke (2008) model predicts the Arago-Rurutu hotspot track trends WNW from Arago seamount (Bonneville et al., 2006), through the region of the Samoan hotspot (Fig. 1). Like the Macdonald hotspot, the Arago-Rurutu hotspot generated HIMU volcanism (e.g. Nakamura & Tatsumoto, 1988; Hauri & Hart, 1993; Chauvel et al., 1997; Bonneville et al., 2006; Jackson et al., 2020). If the HIMU Malulu seamount or the HIMU stage of Papatua seamount formed over the Arago-Rurutu hotspot, they would have predicted ages of \sim 24 to \sim 25 Ma.

Finlayson et al. (2018) and Konrad et al. (2018) picked up the Arago-Rurutu track at East Niulakita (42.24 ± 0.82 Ma- 45.73 ± 0.14 Ma) and Kosciusko $(47.37 \pm 0.11$ Ma $-48.16 \pm$ 0.19 Ma) seamounts near the predicted bend of the hotspot track (i.e., similar morphologically and chronologically to the HEB) (Fig. 1). From there, the track can be traced back to >100 Ma in the Western Pacific (Koppers et al., 2003; Konter et al., 2008; Konrad et al., 2018). However, there is currently no evidence for the Arago-Rurutu hotspot track between Rose atoll (24.81 Ma; Buff et al., 2021) and East Niulakita (45.73 Ma) unless the HIMU portion of Papatua can be determined to be related to the Arago-Rurutu hotspot (Figs 1 and 2). This leaves a \sim 20 Ma gap in volcanism along the Arago-Rurutu hotspot track for which no record has yet been found. Given its radiogenic Pb isotopic composition, Waterwitch seamount was a candidate interloper seamount associated with an origin over the Cook-Austral hotspots (Jackson et al., 2010). However, the robust plagioclase age for Waterwitch presented here $(10.49 \pm 0.09 \text{ Ma})$ falls on the Samoan age progression and indicates a Samoan hotspot origin. The absence of Arago-Rurutu hotspot-derived volcanism in the region between Rose atoll and East Niulakita may relate to two mechanisms. First, Arago-Rurutu volcanoes may be buried under subsequent outpourings of lava associated with more recent passage over the Samoan

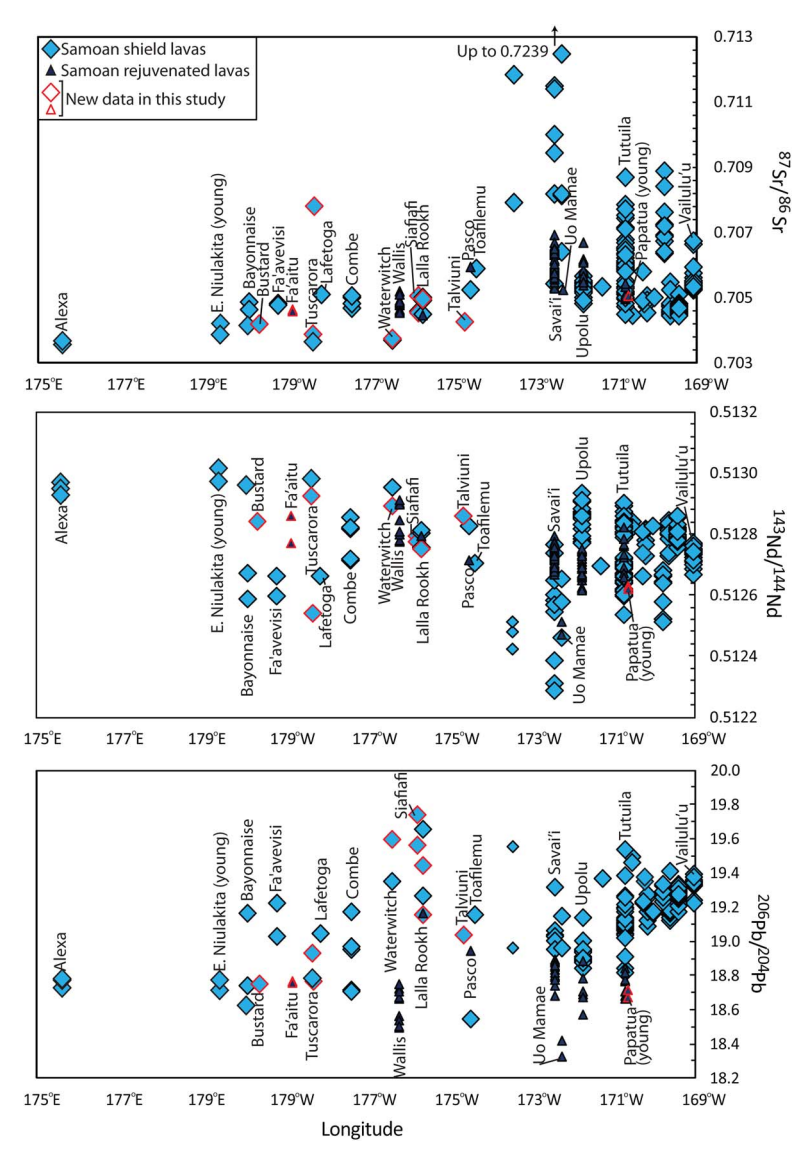


Fig. 5. The ⁸⁷ Sr/⁸⁶ Sr, ¹⁴³ Nd/¹⁴⁴ Nd, and ²⁰⁶ Pb/²⁰⁴ Pb versus longitude of Samoan volcanoes; data for Samoan shield stage and rejuvenated lavas are shown separately. Only the young stages of Papatua and East Niulakita are shown. The non-Samoan interlopers (Rose atoll, Malulu, the older HIMU stage of Papatua, Moki, and the older stage at East Niulakita) are not shown. Samples with red outlines are from this study. The determination of rejuvenated volcanism on the subaerial volcanoes is based on field relationships, but rejuvenated volcanism at submarine locations is based on previously published work that includes a combination of ages and isotopic composition. For example, Hart et al. (2004) suggested sample 3–26 from Lalla Rookh and sample ANT 239-1 from Pasco were rejuvenated based on ages and chemistry. The longitude of each volcano is chosen to be a single value for simplicity. Lead isotope data include only those collected by MC-ICP-MS or double spike TIMS.

hotspot (Finlayson et al., 2018). Indeed, East Niulakita hosts both older HIMU Arago-Rurutu lavas (45.73 Ma) as well as younger Samoan lavas (14.76 Ma) (Finlayson et al., 2018). Alternatively, this portion of the Arago-Rurutu hotspot track may lie further to the south than predicted by the Wessel & Kroenke (2008) model. In this case, the trace of the Arago-Rurutu hotspot would clearly intersect with the northern Tonga trench, with the result being that any Arago-Rurutu hotspot volcanoes erupted between ~25 and ~45 Ma may have been subducted into the trench. This model is consistent with the appearance of HIMU-flavored volcanoes in the northern Lau backarc basin, a possible outcome of subduction of HIMU-related Arago-Rurutu hotspot volcanoes (Falloon et al., 2007; Price et al., 2016, 2017), but may require some

modification to the plate models tested in Finlayson et al. (2018). The WNW striking portion of the Arago-Rurutu hotspot that is older than 45 Ma, and erupted prior to the Arago-Rurutu track bend, escaped subduction because it is located too far north of the northern terminus of the Tonga trench (Fig. 1a); this older portion of the Arago-Rurutu hotspot is traced through the Tuvalu and Gilbert Islands and into the Western Pacific Seamount Province (Koppers et al., 2003; Konter et al., 2008; Konrad et al.,

Additionally at present, the portion of the Arago-Rurutu hotspot between Aitutaki and Rose remains unsampled, and numerous seamounts between Aitutaki and Rose present targets that could potentially close this gap in the Arago-Rurutu hotspot.

Rarotonga group

Due to the lack of any known, age-progressive track linked to the active melt zone, Rarotonga is unlikely to be an authentic hotspot (Jackson et al., 2020). Instead, the entire "hotspot track" is defined by overlapping periods of volcanism at just two volcanoes spaced only ~260 km apart: Rarotonga (1.157–1.697 Ma) and the young stage of Aitutaki (1.382-1.941 Ma) (Rose & Koppers, 2019), which are located over 1200 km east-southeast of Papatua and have EM1 isotopic compositions. Indeed, Chauvel et al. (1997) noted that the Rarotonga hotspot is "less well expressed" than the other hotspots in the Cook-Austral Volcanic Lineament. No age-progressive volcanoes associated with this "hotspot" have been identified west of Rarotonga and Aitutaki islands. Unless Rarotonga is the product of a relatively new hotspot that only became active over the last few million years—which might explain the lack of a long-term age progression that can be traced to the WNW of Rarotonga Island—there is no evidence of a hotspot origin for Rarotonga Island and the young stage of Aitutaki (Jackson et al., 2020). For this reason, we designate Rarotonga as a volcanic "group" rather than a hotspot track and we do not consider it to be responsible for volcanism at Papatua.

Samoan hotspot

The westernmost known expression of the Samoan hotspot is Alexa bank (Figs 1 and 2), with an age of 23.96 Ma (Hart et al., 2004). However, the geochemistry of Alexa bank exhibits radiogenic isotopic compositions that are unusually depleted (i.e., 87 Sr/86 Sr < 0.7044) relative to other known Samoan shield lavas (referred hereafter as Alexa-type). Finlayson et al. (2018) showed that Samoan shield lavas with depleted radiogenic isotopic signatures are not unique to Alexa bank and they characterized other WESAM volcanoes along the Samoan hotspot track, including Tuscarora, Bayonnaise, and Samoan lavas from East Niulakita. The Tuscarora bank clasts and Bustard lava studied here both have compositions similar to those of the geochemically depleted Alexa-type lavas (although Bustard is slightly more geochemically enriched) (Fig. 4). These lavas support the hypothesis that Samoan lavas with depleted radiogenic isotopic signatures are located widely along the WESAM region of the Samoan hotspot track (a span of ~640 km from Alexa bank to Tuscarora seamount), but not in the ESAM region (Fig. 5): there are no volcanoes east of Savai'i with ⁸⁷Sr/⁸⁶Sr < 0.7044, but eight Samoan volcanoes with 87Sr/86Sr < 0.7044 are identified west of Savai'i (nine if Nukulaelae is included as a Samoan volcano; Finlayson et al., 2018). Furthermore, the basaltic clast sample from Tuscarora bank (KK8203-DR-9) has much lower 87 Sr/ 86 Sr (0.703789) than the other Tuscarora bank lava in this study (see sample RR1310-D34-01 [with 87 Sr/ 86 Sr = 0.707822]), indicating that Samoan lavas with depleted Alexa-type geochemistry and normal Samoan shield geochemistry can be found at the same volcano.

Several WESAM lavas from this study (e.g. Lalla Rookh, Siafiafi, Talviuni, and the Tuscarora bank lava) show moderately enriched isotopic signatures that plot close to or within the range of previously published Samoan shield lavas (Fig. 4). Our new geochemical and age data on sample RR1310-D38-08 suggests that Waterwitch seamount, which was previously grouped with non-Samoan "interlopers" based on the radiogenic isotopic composition of one lava (ALIA-D122-03; Jackson et al., 2010), is in fact Samoan. Therefore, the field for Samoan shield lavas in radiogenic isotopic space should be enlarged to include Waterwitch, which has relatively high ²⁰⁶Pb/²⁰⁴Pb (19.35-19.60), and plots outside the previously known range identified for other Samoan shield volcanoes (Fig. 4).

We also note that it is unlikely that the apparently older HIMU stage found at Papatua seamount was generated over the Samoan hotspot. First, the ferromanganese rind on the HIMU Papatua sample ALIA-D129-05 (>5 cm) is much thicker than the rinds, or patinas, from young Samoan volcanoes in the vicinity (<1 mm). Second, the HIMU Pb isotopic composition (206 Pb/ 204 Pb = 20.0) of the Papatua seamount lava is significantly more radiogenic than that found in Samoan lavas (Fig. 4). Workman et al. (2004) suggested that the slightly more radiogenic Pb isotopes in the youngest, easternmost volcanoes along the Samoan hotspot may be a result of the Pacific plate acquiring this signature during prior passage of this region of the Pacific plate over the HIMU Cook-Austral hotspots, Arago-Rurutu, and Macdonald. In this scenario, this region of Pacific lithosphere, which had previously been underplated by HIMU Cook-Austral material, rafted into the Samoan hotspot region with plate motion, which then became incorporated into the upwelling Samoan plume (or Samoan plume melts). However, the extreme HIMU signatures present in the Cook-Australs are not observed in Samoa, and Jackson et al. (2014) showed that the milder HIMU signatures in some Samoan hotspot volcanoes can also be explained as being part of the Samoan plume.

Anomalously young volcanism along the Samoan hotspot track

In contrast to the apparently old and visually altered Papatua sample ALIA-D129-05, the two pristine Papatua glasses studied here were dredged at shallower depths (2000 mbsl) on the seamount, presumably sampling stratigraphically higher, and younger, material. These Papatua glass samples were attached to extremely fresh mantle xenoliths that were the subject of Poreda & Farley's (1992) rare gas study. Peridotite mantle xenoliths associated with the Samoan hotspot have only been reported in rejuvenated lavas (e.g. Natland, 1980; Hauri & Hart, 1994), and while Poreda & Farley (1992) did not publish the major and trace element, or isotopic compositions measured in the host glass, they did note that "the chemical and Sr-Nd isotopic compositions of the Si-undersaturated glass ... leave little doubt that they were erupted by post-erosional stage volcanics."

The new geochemical data presented herein on these glasses support Poreda & Farley's (1992) interpretation: the Papatua lavas are Si undersaturated and plot in or on the fringes of the Samoan rejuvenated field in all isotope spaces except for that of Hf-Nd (but this may be due to a paucity of Hf isotope data for Samoan rejuvenated lavas) (Fig. 4). We find that the two Papatua glasses have EM1 compositions, a geochemical signature associated with rejuvenated volcanism along the nearby Samoan hotspot track, which contrasts with the HIMU compositions identified in the more deeply dredged, ferromanganese-encrusted Papatua sample ALIA-D129-05. Both glasses appear extremely fresh, lacking visible signs of alteration or ferromanganese encrustation. As volcanic glass and peridotite xenoliths weather rapidly in submarine conditions, the pristine nature of the Papatua glasses supports the interpretation that they are relatively young, which is inconsistent with the old age inferred for the HIMU Papatua lava (ALIA-D129-05). These differences in isotopic composition and apparent age suggest that Papatua erupted both an older HIMU stage sampled by ALIA-D129-05 and an EM1 stage inferred by Poreda & Farley (1992) to represent rejuvenated-stage volcanism. Furthermore, extreme EM1 volcanism on the nearby Uo Mamae seamount (Figs 2 and 4) has been suggested to relate to Samoan rejuvenated volcanism (e.g. Regelous et al., 2008). If the Samoan rejuvenated field in radiogenic isotope space is expanded to include Samoan rejuvenated lavas sensu stricto as well as Uo Mamae lavas, the field encompasses Papatua rejuvenated lavas (Fig. 4), suggesting a common mantle source for the EM1 Papatua and Samoan rejuvenated lavas.

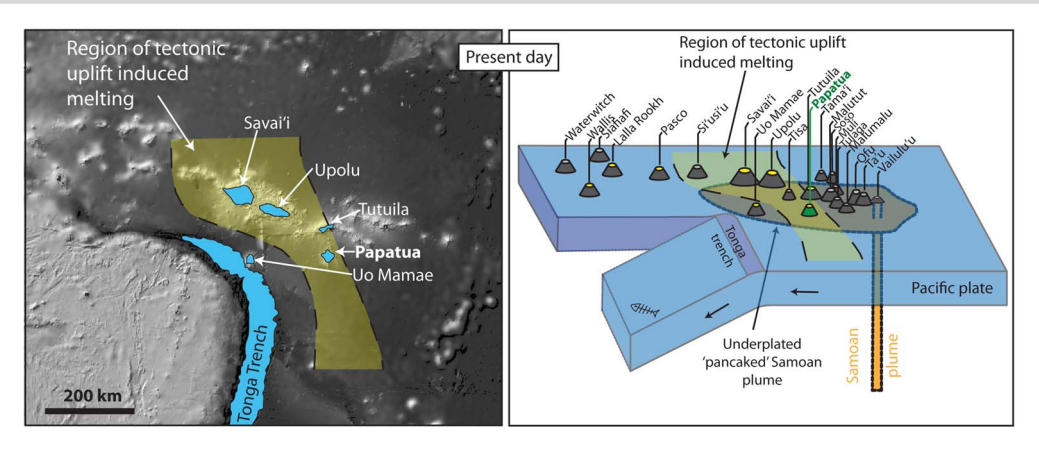
Young, rejuvenated lavas with EM1 signatures are found capping ESAM shield volcanoes on nearby Tutuila, Upolu, and Savai'i (e.g. Hawkins & Natland, 1975; Natland & Turner, 1985; Hauri & Hart, 1993; Natland, 2003; Workman et al., 2004; Konter & Jackson, 2012). However, several WESAM volcanoes also appear to host anomalously young volcanism. For example, Hart et al. (2004) found that a sample from Lalla Rookh seamount (located ~725 km west of Vailulu'u) erupted a much younger rejuvenated lava (1.63 \pm 0.06 Ma), which falls off the Samoan age progression (Fig. 1b). Lavas from Wallis Island, located ∼70 km southwest of Lalla Rookh seamount, are also young (0.08 Ma, Price et al., 1991) and geochemically consistent with rejuvenated lavas from Samoa (Price et al., 2014). Our 40 Ar/39 Ar ages show that one Bustard lava (3.47 \pm 0.02 Ma), located \sim 1170 km west of Vailulu'u, as well as two Fa'aitu seamount lavas $(1.26 \pm 0.14 \text{ Ma} \text{ and } 1.48 \pm 0.19 \text{ Ma}) \text{ located } \sim 1050 \text{ km}$ west of Vailulu'u, are each ~10 million years younger than expected from a Samoan age progression (Fig. 1b). The two lavas from Fa'aitu show weak EM1 signatures and plot within or close to the field for Samoan rejuvenated lavas in Pb-Sr-Nd isotope space (Fig. 4), so their young ages and geochemistry are permissive of an origin similar to Samoan rejuvenated lavas.

Unfortunately, the single geochemically characterized Bustard lava (RR1310-D29-10) does not have an available age, and the 3.47 Ma Bustard lava is not geochemically characterized. The RR1310-D29-10 lava has Alexatype geochemistry that differs from most rejuvenatedstage Samoan lavas, but the young age of the Bustard lava RR1310-D29-01 supports the interpretation that it represents rejuvenated volcanism. However, the origin of the anomalously young volcanism in the WESAM remains unclear.

Exploring causes of rejuvenated volcanism along the Samoan hotspot track

Regelous et al. (2008) argued that the extreme radiogenic isotopic compositions found at Uo Mamae reflect an endmember that contributes to rejuvenated volcanism in Samoa. Hawkins & Natland (1975) also noted that a young lava (0.94 Ma) dredged from the summit of Uo Mamae may be rejuvenated, and Regelous et al. (2008) suggested that it may have formed as the volcano underwent extensional faulting while approaching the Tonga trench. In fact, it has been shown that Samoan mantle material is sampled not only by Uo Mamae, but also by Tafahi and Niuatoputapu, northern Tonga arc islands located, respectively, \sim 280 and \sim 300 km south of the trace of the Samoan hotspot track, as well as lavas in the northern Lau basin located further to the west (e.g. Wendt et al., 1997; Turner & Hawkesworth, 1998; Regelous et al., 2008; Zhang et al., 2019) (Fig. 2). If Samoan-type mantle has also pervaded the region beneath Papatua, which is located only ~60 km south of Tutuila Island—a Samoan hotspot volcano that has erupted EM1 rejuvenated lavas in the past 24 000 years (Reinhard et al., 2019)—it is possible that the EM1 rejuvenated lavas on Papatua are also geochemically influenced by Samoan material. However, while the composition of the apparently young EM1 Papatua glasses suggests a genetic link to Samoan rejuvenated volcanoes and is therefore inferred to be young—the HIMU portion of the Papatua seamount (206 Pb/ 204 Pb = 20.0) is clearly not Samoan and likely relates to much older volcanism associated with prior passage over one of the Cook-Austral hotspots. This raises a key question: How can Samoan rejuvenated lavas manifest at a non-Samoan volcano?

It has been suggested that tectonic stresses produced flexural uplift in the Pacific plate near the northern terminus of the Tonga trench, where the Pacific plate is tearing and the southern portion is subducting (e.g. Hawkins & Natland, 1975; Natland, 1980; Levitt & Sandwell, 1995; Millen & Hamburger, 1998; Govers & Wortel, 2005). This uplift may trigger mantle melting that taps EM1-material giving rise to rejuvenated lavas capping Samoa shield volcanoes (e.g. Price et al., 1991; Hart et al., 2004; Konter & Jackson, 2012). Savai'i, the Samoan island with the most extensive rejuvenated volcanism, lies ~130 km north of the northern terminus of the Tonga trench, and both the extent of rejuvenated volcanism and the proximity to the trench suggest a tectonic trigger for rejuvenation



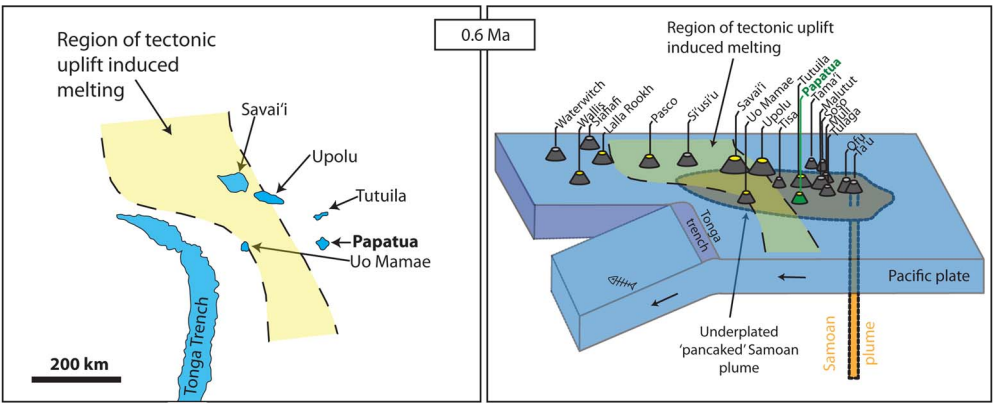


Fig. 6. Regional tectonic model for rejuvenated volcanism. Maps show the evolution of the Samoan hotspot region at 0.6 Ma and the present day. The plate reconstruction is based on Koppers et al. (2008), Ruellan et al. (2003), and Hart et al. (2004). The yellow shaded area shows the region where upward plate velocity is >0.4 mm/year and is based on the finite difference model of Govers & Wortel (2005) and follows Konter & Jackson (2012). Volcanoes with a known Samoan origin have gray "bases". The "base" of Papatua seamount, which may originate from either of the two upstream HIMU hotspots—Arago-Rurutu or Macdonald (but not Samoa)—is green. Volcanoes with yellow-colored "tops" indicate the presence of Samoan EM1 rejuvenated lavas on that volcano (including Lalla Rookh, Pasco, and Wallis, which have ages and/or geochemical signatures that support a rejuvenated stage). Dead fish, from the inspirational figure of Natland (1980), marks the westward subduction of the Pacific plate. The Tonga trench has moved to the east over the past 0.6 Ma, while the Samoan volcanoes have moved westward on the Pacific plate. In our cartoon, Ta'u island, which was active from 0.02 to 0.7 Ma, is located atop the Samoan plume at the 0.6 Ma time step.

(e.g. Hawkins & Natland, 1975; Koppers et al., 2008, 2011; Konter & Jackson, 2012).

Lithospheric deformation of the Pacific plate outboard of the northern Tonga Trench was modeled using a 3D numerical model by Govers & Wortel (2005), which serves as the basis for the "region of flexural uplift" in Fig. 6. Konter & Jackson (2012) created a quantitative model to show how this flexural uplift generates decompression melting that can explain rejuvenated volcanism in the Samoan region. In detail, Konter & Jackson (2012) explored the possible link between the timing of the onset of rejuvenated volcanism in the ESAM to a volcano's approach to the trench, first on Savai'i (which is located closer to the trench) and then on Tutuila (which is further from the trench). In this scenario, melting initiates during the Pacific plate's approach to the trench when the plate enters a region of flexuredriven uplift at a rate of ~0.4 mm/year (Fig. 6; based on Govers & Wortel (2005), Konter & Jackson (2012), and Reinhard et al. (2019)). To illustrate how Samoan volcanoes move into this region of high flexural uplift as the Pacific plate approaches the trench, two time-steps are shown in Fig. 6: 0.6 Ma and present day. Reinhard

et al. (2019) showed that the region of high flexural uplift is associated with recent rejuvenated volcanism in the Samoan regio including volcanism at Uo Mamae, Savai'i, Upolu, and Tutuila. Papatua moved into this region of tectonically induced melting between 0.6 Ma and the present day. Critically, Papatua seamount is currently located only \sim 200 km east-northeast of the northern terminus of the Tonga trench—similar to the distance between Tutuila and the trench—suggesting that the same tectonic stresses that trigger rejuvenated volcanism in the Samoan region might arguably also affect nearby Papatua seamount (see Fig. 6). Because Tutuila and Papatua would have crossed into the region of high flexural uplift at a similar time, and because the initiation of rejuvenated volcanism occurred at 24 ka on Tutuila (Reinhard et al., 2019), tectonically triggered rejuvenated volcanism at Papatua might also have been initiated recently. In this scenario, the tectonic forces from the nearby trench triggered recent rejuvenated melting of underplated Samoan mantle material that had flowed southward under Papatua. The southward flow of the Samoan material toward Papatua could be facilitated by the plume spreading out laterally and flattening, or "pancaking", as it rises and impinges on the base of the Pacific lithosphere (Phipps Morgan et al., 1995), thereby explaining the presence of Samoan plume material beneath a non-Samoan volcano (Papatua seamount) located ~60 km south of the Samoan hotspot track (Fig. 6). Thus, this simple process of tectonically triggered melting of southward advected Samoan plume material helps explain both the Samoan EM1 geochemistry and the apparent young age of the rejuvenated volcanic glasses along with older, non-Samoan HIMU lavas at Papatua seamount.

Similar to rejuvenated volcanism occurring off the axis of the Samoan hotspot at Papatua, secondary offshore volcanism at Hawai'i has also been linked to flexural uplift (e.g. Lipman et al., 1989; Frey, 2000). Modeling of flexural uplift surrounding a growing volcanic shield shows this to trigger decompression of mantle plume material (Bianco et al., 2005). The material, which initially partially melted under the shield volcano, then flowed out laterally. This model is supported at Hawai'i by the secondary volcanism at the South Arch Volcanic Field, located ~200 km south of Lō'ihi seamount (e.g. Lipman et al., 1989). Additionally, rejuvenated lavas and "petitspot" lavas form by similar processes (lithosphere uplift and decompression), and Reinhard et al. (2019) found that petit spot volcanoes also have clear geochemical similarities (e.g. strong EM1 affinities) with Samoan rejuvenated volcanism.

In a similar vein, tectonic reactivation may also explain young volcanism in the WESAM. Utilizing a variety of geophysical data, Pelletier & Auzende (1996) determined that the WESAM region south of East Niulakita has experienced relatively recent extension and normal faulting in the region near the Vitiaz lineament. In addition to a 0.2 Ma age basalt recovered near Bayonnaise, they interpreted cone-shaped edifices as recent volcanism that was synchronous with or immediately post-dating this normal faulting. Bustard (3.47 Ma) and Fa'aitu (1.26–1.48 Ma) seamounts are located just south of East Niulakita in the region impacted by recent extension. We therefore consider that tectonic reactivation allowed EM1 melts in the shallow mantle to erupt and form the young lavas found on Bustard and Fa'aitu, long after these volcanoes passed over the Samoan hotspot. Like Fa'aitu, Wallis (0.08 Ma; Price et al., 1991) is located near the Vitiaz lineament, and Lalla Rookh (1.6 Ma; Hart et al., 2004) is only 100 km north of the Vitiaz lineament. If there has been wide-scale extension in the region of the Vitiaz between Wallis and Fa'aitu over the past 3.5 Ma, it may explain exceptionally young volcanism at all four WESAM volcanoes: Lalla Rookh, Wallis, Fa'aitu, and Bustard.

The prospect of Cretaceous Samoan volcanism

Looking beyond Alexa, it is possible that the Samoan hotspot track may extend back into the Cretaceous (e.g. Koppers et al., 1998, 2003). The Wessel & Kroenke (2008) plate motion model places the HEB-like bend of the Samoan chain beneath the Ontong Java Plateau, which may have suppressed volcanism in the region due to its substantially increased lithospheric thickness. However, 100 Ma-old seamounts located in the southern portion of the Western Pacific Seamount Province, north of the Ontong Java Plateau, have ages and geochemistry consistent with an origin over the Samoan hotspot (e.g. Koppers et al., 2003; Konter et al., 2008). Future expeditions sampling the possible trace of the hotspot prior to 25 Ma are warranted.

CONCLUSIONS

40 Ar/39 Ar data provide additional constraints on the make-up of the "hotspot highway" along the Samoan hotspot track. Based on a 40 Ar/ 39 Ar age of 10.49 \pm 0.09 Ma for Waterwitch, this seamount falls on the Samoan age progression, consistent with a Samoan origin. This contrasts with a previous suggestion that Waterwitch is a HIMU "interloper" volcano left over from passage of the Pacific lithosphere over the Cook-Austral hotspots. This finding implies a paucity of HIMU-interlopers west of Papatua seamount, which may be related to subduction of Cook-Austral-related seamounts into the northern Tonga trench, or burial of old Cook-Austral volcanoes under the lava piles of more recently generated Samoan hotspot volcanoes.

It appears that Papatua seamount underwent at least two stages of volcanism, including a HIMU stage (related to prior passage over either the Arago-Rurutu or Macdonald hotspots at ~25 or ~44 Ma, respectively), and a younger EM1 stage of rejuvenated volcanism. The EM1 Papatua glasses are geochemically similar to EM1-rejuvenated lavas found in Samoa and Uo Mamae seamount, which leads us to suggest that these EM1 stages at Papatua may relate to Samoan rejuvenated volcanism, which is pervasive in the Samoan region. Flexural uplift in the Pacific plate near the northern terminus of the Tonga trench results in melting of southward advected Samoan plume material that ultimately erupts at Papatua.

Lastly, 40 Ar/39 Ar ages for Fa'aitu seamount lavas highlight the presence of exceptionally young volcanism (<3.5 Ma) of unknown origin in the WESAM region. This unusual volcanism may relate to regional tectonic reactivation along the Vitiaz lineament, which allowed melts in the shallow mantle to erupt and form the young lavas long after the volcano passed over the Samoan hotspot.

FUNDING

MGJ acknowledges funding from National Science Foundation grants OCE-1929095, OCE-1912931, OCE-1736984, and EAR-1429648. JBT acknowledges funding from the French Agence Nationale de la Recherche

(grant ANR-10-BLANC-0603 M&Ms-Mantle Melting-Measurements, Models, Mechanisms). JK acknowledges National Science Foundation grant OCE 1912934.

SUPPLEMENTARY DATA

Supplementary data are available at Journal of Petrology online.

ACKNOWLEDGMENTS

We thank Ken Farley for providing the Papatua glasses and Stan Hart and Hubert Staudigel for providing a sample from the 2005 Samoa ALIA cruise. We also acknowledge Stan Hart for inspiring us to target the glasses on the Papatua xenoliths for isotope work. We also thank Marcel Regelous and an anonymous reviewer for their helpful comments. The data underlying this article are available in tables within the article.

References

- Adams, J. V., Jackson, M. G., Spera, F. J., Price, A. A., Byerly, B. L., Seward, G. & Cottle, J. M. (2021). Extreme isotopic heterogeneity in Samoan clinopyroxenes constrains sediment recycling. Nature Communications 12(1), 1-10.
- Bianco, T. A., Ito, G., Becker, J. M. & Garcia, M. O. (2005). Secondary Hawaiian volcanism formed by flexural arch decompression. Geochemistry, Geophysics, Geosystems 6(8), Q08009. https://doi. org/10.1029/2005GC000945.
- Becker, J. J., Sandwell, D. T., Smith, W. H. F., Braud, J., Binder, B., Depner, J. L., Fabre, D., Factor, J., Ingalls, S., Kim, S. H. & Ladner, R. (2009). Global bathymetry and elevation data at 30 arc seconds resolution: SRTM30_PLUS. Marine Geodesy 32(4), 355-371.
- Béguelin, P., Bizimis, M., Beier, C. & Turner, S. (2017). Rift-plume interaction reveals multiple generations of recycled oceanic crust in Azores lavas. Geochimica et Cosmochimica Acta 218, 132-152.
- Blichert-Toft, J. & Albarède, F. (2009). Mixing of isotopic heterogeneities in the Mauna kea plume conduit. Earth and Planetary Science Letters 282(1), 190-200.
- Blichert-Toft, J., Chauvel, C. & Albarède, F. (1997). Separation of Hf and Lu for high-precision isotope analysis of rock samples by magnetic sector-multiple collector ICP-MS. Contributions to Mineralogy and Petrology 127(3), 248-260.
- Bonneville, A., Le Suavé, R., Audin, L., Clouard, V., Dosso, L., Gillot, P. Y., Janney, P., Jordahl, K. & Maamaatuaiahutapu, K. (2002). Arago seamount: the missing hotspot found in the Austral Islands. Geology 30(11), 1023-1026.
- Bonneville, A., Dosso, L. & Hildenbrand, A. (2006). Temporal evolution and geochemical variability of the South Pacific superplume activity. Earth and Planetary Science Letters 244, 251–269.
- Buff, L., Jackson, M. G., Konrad, K., Konter, J. G., Bizimis, M., Price, A., Rose-Koga, E. F., Blusztajn, J., Koppers, A. A. P. & Herrera, S. (2021). "Missing links" for the long-lived Macdonald and Arago hotspots, South Pacific Ocean. Geology 49(5), 541-544.
- Chauvel, C., McDonough, W., Guille, G., Maury, R. & Duncan, R. (1997). Contrasting old and young volcanism in Rurutu Island, Austral chain. Chemical Geology 139(1-4), 125-143.
- Diraison, C. (1991) Le volcanisme aérien des archipels polynésiens de la Société, des Marquises et des Australes-Cook. Téphrostratigraphie, datation isotopique et géochimie comparées. In: Contribution à l'étude des origines du volcanisme intraplaque du Pacifique Central.

- Thèse de Doctorat, Univ. Bretagne Occidentale, Brest, p.413 dissertation.
- Duncan, R. A. (1985). Radiometric ages from volcanic rocks along the New Hebrides-Samoa lineament. Investigations of the Northern Melanesian Borderland, Circum-Pacific Council for Energy and Mineral Resources. Earth Science Series, Vol. 3. pp. 67–75. Circum-Pacific Council for Energy and Mineral Resources, Houston, Texas.
- Duncan, R. A. & McDougall, I. (1976). Linear volcanism in French Polynesia. Journal of Volcanology and Geothermal Research 1(3), 197-227.
- Eisele, J., Abouchami, W., Galer, S. J. & Hofmann, A. W. (2003). The 320 kyr Pb isotope evolution of Mauna Kea lavas recorded in the HSDP-2 drill core. Geochemistry, Geophysics, Geosystems 4(5),
- Falloon, T. J., Danyushevsky, L. V., Crawford, T. J., Maas, R., Woodhead, J. D., Eggins, S. M., Bloomer, S. H., Wright, D. J., Zlobin, S. K. & Stacey, A. R. (2007). Multiple mantle plume components involved in the petrogenesis of subduction-related lavas from the northern termination of the Tonga Arc and northern Lau Basin: evidence from the geochemistry of arc and backarc submarine volcanics. Geochemistry, Geophysics, Geosystems 8(9), Q09003. https://doi.org/10.1029/2007GC001619.
- Finlayson, V. A., Konter, J. G., Konrad, K., Koppers, A. A. P., Jackson, M. G. & Rooney, T. O. (2018). Sr-Pb-Nd-Hf isotopes and 40 Ar/39 Ar ages reveal a Hawaii–Emperor-style bend in the Rurutu hotspot. Earth and Planetary Science Letters 500, 168-179.
- Frey, F. A. (2000). Volcanism at the edge of the Hawaiian plume: petrogenesis of submarine alkalic lavas from the North Arch volcanic field. Journal of Petrology 41, 667-691.
- Gagnon, J. E., Fryer, B. J., Samson, I. M. & Williams-Jones, A. E. (2008). Quantitative analysis of silicate certified reference materials by LA-ICPMS with and without an internal standard. Journal of Analytical Atomic Spectrometry 23(11), 1529-1537.
- Gale, A., Dalton, C. A., Langmuir, C. H., Su, Y. & Schilling, J. G. (2013a). The mean composition of ocean ridge basalts. Geochemistry, Geophysics, Geosystems 14, 489-518.
- Gale, A., Laubier, M., Escrig, S. & Langmuir, C. H. (2013b). Constraints on melting processes and plume-ridge interaction from comprehensive study of the FAMOUS and North Famous segments, Mid-Atlantic Ridge. Earth and Planetary Science Letters 365, 209-220.
- Garçon, M., Boyet, M., Carlson, R. W., Horan, M. F., Auclair, D. & Mock, T. D. (2018). Factors influencing the precision and accuracy of Nd isotope measurements by thermal ionization mass spectrometry. Chemical Geology 476, 493–514.
- Govers, R. & Wortel, M. J. R. (2005). Lithosphere tearing at STEP faults: response to edges of subduction zones. Earth and Planetary Science Letters 236(1-2), 505-523.
- Hart, S. & Blusztajn, J. (2006). Age and geochemistry of the mafic sills, ODP site 1276, Newfoundland margin. Chemical Geology 235, 222-237.
- Hart, S. R., Staudigel, H., Koppers, A. A., Blusztajn, J., Baker, E. T., Workman, R., Jackson, M., Hauri, E., Kurz, M., Sims, K. & Fornari, D. (2000). Vailulu'u undersea volcano: the new Samoa. Geochemistry, Geophysics, Geosystems 1(12), 1056.
- Hart, S. R., Coetzee, M., Workman, R. K., Blusztajn, J., Johnson, K. T. M., Sinton, J. M., Steinberger, B. & Hawkins, J. W. (2004). Genesis of the Western Samoa seamount province: age, geochemical fingerprint and tectonics. Earth and Planetary Science Letters 227(1), 37–56.
- Hauri, E. H. & Hart, S. R. (1994). Constraints on melt migration from mantle plumes: a trace element study of peridotite xenoliths from Savai'i, Western Samoa. Journal of Geophysical Research: Solid Earth 99(B12), 24301–24321.

- Hauri, E. K. & Hart, S. R. (1993). ReOs isotope systematics of HIMU and EMII oceanic island basalts from the south Pacific Ocean. Earth and Planetary Science Letters 114(2), 353-371.
- Hawkins, J. W. & Natland, J. (1975). Nephelinites and basanites of the Samoan linear volcanic chain: their possible tectonic significance. Earth and Planetary Science Letters 24(3), 427-439.
- Jackson, M. G., Kurz, M. D., Hart, S. R. & Workman, R. K. (2007a). New Samoan lavas from Ofu Island reveal a hemispherically heterogeneous high 3He/4He mantle. Earth and Planetary Science Letters **264**(3-4, 374), 360.
- Jackson, M. G., Hart, S. R., Koppers, A. A., Staudigel, H., Konter, J., Blusztajn, J., Kurz, M. & Russell, J. A. (2007b). The return of subducted continental crust in Samoan lavas. Nature 448(7154), 684-687.
- Jackson, M. G., Hart, S. R., Konter, J. G., Koppers, A. A., Staudigel, H., Kurz, M. D., Blusztajn, J. & Sinton, J. M. (2010). Samoan hot spot track on a "hot spot highway": implications for mantle plumes and a deep Samoan mantle source. Geochemistry, Geophysics, Geosystems 11, Q12009.
- Jackson, M. G., Hart, S. R., Konter, J. G., Kurz, M. D., Blusztajn, J. & Farley, K. A. (2014). Helium and lead isotopes reveal the geochemical geometry of the Samoan plume. Nature 514, 355-358.
- Jackson, M. G., Koga, K. T., Price, A., Konter, J. G., Koppers, A. A., Finlayson, V. A., Konrad, K., Hauri, E. H., Kylander-Clark, A., Kelley, K. A. & Kendrick, M. A. (2015). Deeply dredged submarine HIMU glasses from the Tuvalu Islands, Polynesia: implications for volatile budgets of recycled oceanic crust. Geochemistry, Geophysics, Geosystems 16(9), 3210-3234.
- Jackson, M. G., Price, A. A., Blichert-Toft, J., Kurz, M. D. & Reinhard, A. A. (2017). Geochemistry of lavas from the Caroline hotspot, Micronesia: evidence for primitive and recycled components in the mantle sources of lavas with moderately elevated ³He/⁴He. Chemical Geology 455, 385-400.
- Jackson, M. G., Halldórsson, S. A., Price, A., Kurz, M. D., Konter, J. G., Koppers, A. A. P. & Day, J. M. D. (2020). Contrasting old and young volcanism from Aitutaki, Cook Islands: implications for the origins of the cook-austral volcanic chain. Journal of Petrology 61(3), egaa037.
- Jochum, K. P., Stoll, B., Herwig, K., Willbold, M., Hofmann, A. W., Amini, M., Aarburg, S., Abouchami, W., Hellebrand, E., Mocek, B. & Raczek, I. (2006). MPI-DING reference glasses for in situ microanalysis: new reference values for element concentrations and isotope ratios. Geochemistry, Geophysics, Geosystems 7(2), Q02008. https:// doi.org/10.1029/2005GC001060.
- Jochum, K. P., Weis, U., Schwager, B., Stoll, B., Wilson, S. A., Haug, G. H., Andreae, M. O. & Enzweiler, J. (2016). Reference values following ISO guidelines for frequently requested rock reference materials. Geostandards and Geoanalytical Research 40(3), 333-350.
- Johnson, K. T. M. & Sinton, J. M. (1990). Petrology, tectonic setting, and the formation of back-arc basin basalts in the North Fiji Basin. Geologisches Jahrbuch Reihe D Heft, Vol. 92. pp. 517-545.
- Johnson, K. T. M., Sinton, J. M. & Price, R. C. (1986). Petrology of seamounts northwest of Samoa and their relation to Samoan volcanism. Bulletin of Volcanology 48, 225-235.
- Knaack, C., Cornelius, S. & Hooper, P. R. (1994) Trace element analyses of rocks and minerals by ICP-MS. In: Open File Report. Pullman, Washington: Department of Geology, Washington State Univer-
- Konrad, K., Koppers, A. A., Steinberger, B., Finlayson, V. A., Konter, J. G. & Jackson, M. G. (2018). On the relative motions of long-lived Pacific mantle plumes. Nature Communications 9(1), 1-8.
- Konter, J. G. & Jackson, M. G. (2012). Large volumes of rejuvenated volcanism in Samoa: evidence supporting a tectonic influence

- on late-stage volcanism. Geochemistry, Geophysics, Geosystems 13, O0AM04.
- Konter, J. G. & Storm, L. P. (2014). High precision 87 Sr/86 Sr measurements by MC-ICP-MS, simultaneously solving for Kr interferences and mass-based fractionation. Chemical Geology 385, 26-34.
- Konter, J. G., Hanan, B. B., Blichert-Toft, J., Koppers, A. A., Plank, T. & Staudigel, H. (2008). One hundred million years of mantle geochemical history suggest the retiring of mantle plumes is premature. Earth and Planetary Science Letters 275(3-4), 285-295.
- Koppers, A. A. (2002). ArArCALC—software for 40 Ar/39 Ar age calculations. Computers & Geosciences 28(5), 605-619.
- Koppers, A. A., Staudigel, H., Wijbrans, J. R. & Pringle, M. S. (1998). The Magellan seamount trail: implications for Cretaceous hotspot volcanism and absolute Pacific plate motion. Earth and Planetary Science Letters 163(1-4), 53-68.
- Koppers, A. A., Staudigel, H., Pringle, M. S. & Wijbrans, J. R. (2003). Short-lived and discontinuous intraplate volcanism in the South Pacific: hot spots or extensional volcanism? Geochemistry, Geophysics, Geosystems 4(10), 1089.
- Koppers, A. A., Staudigel, H., Phipps Morgan, J. & Duncan, R. A. (2007). Nonlinear 40 Ar/39 Ar age systematics along the Gilbert Ridge and Tokelau Seamount Trail and the timing of the Hawaii-Emperor Bend. Geochemistry, Geophysics, Geosystems 8(6), Q06L13. https:// doi.org/10.1029/2006GC001489.
- Koppers, A. A., Russell, J. A., Jackson, M. G., Konter, J., Staudigel, H. & Hart, S. R. (2008). Samoa reinstated as a primary hotspot trail. Geology 36(6), 435-438.
- Koppers, A. A., Russell, J. A., Roberts, J., Jackson, M. G., Konter, J. G., Wright, D. J., Staudigel, H. & Hart, S. R. (2011). Age systematics of two young en echelon Samoan volcanic trails. Geochemistry, Geophysics, Geosystems 12, Q07025.
- Kuiper, K. F., Deino, A., Hilgen, F. J., Krijgsman, W., Renne, P. R. & Wijbrans, A. J. (2008). Synchronizing rock clocks of earth history. Science 320(5875), 500-504.
- Le Bas, M. J., Maitre, R. L., Streckeisen, A. & Zanettin, B. (1986). A chemical classification of volcanic rocks based on the total alkalisilica diagram. Journal of Petrology 27(3), 745-750.
- Levitt, D. A. & Sandwell, D. T. (1995). Lithospheric bending at subduction zones based on depth soundings and satellite gravity. Journal of Geophysical Research: Solid Earth 100(B1), 379–400.
- Lipman, P. W., Clague, D. A., Moore, J. G. & Holcomb, R. T. (1989). South Arch volcanic field—newly identified young lava flows on the sea floor south of the Hawaiian Ridge. Geology 17(7), 611-614.
- MacDonald, G. A. & Katsura, T. (1964). Chemical composition of Hawaiian lavas. Journal of Petrology 5(1), 82-133.
- Matsuda, J. I., Notsu, K., Okano, J., Yaskawa, K. & Chungue, L. (1984). Geochemical implications from Sr isotopes and K-Ar age determinations for the Cook-Austral Islands chain. Tectonophysics 104(1-2), 145-154.
- Maury, R. C., Guille, G., Guillou, H., Chauvel, C., Rossi, P., Pallares, C. & Legendre, C. (2013). Temporal evolution of a Polynesian hotspot: new evidence from Raivavae (Austral islands, South Pacific Ocean). Bulletin de la Société Géologique de France 184(6), 557-567.
- McDonough, W. F. & Sun, S. S. (1995). The composition of the earth. Chemical Geology 120(3-4), 223-253.
- McDougal, I. (2010). Age of volcanism and its migration in the Samoa Islands. Geological Magazine 147(5), 705–717.
- McNutt, M. K., Caress, D. W., Reynolds, J., Jordahl, K. A. & Duncan, R. A. (1997). Failure of plume theory to explain midplate volcanism in the southern Austral islands. Nature 389(6650), 479-482.

- Melson, W. G., O'Hearn, T. & Jarosewich, E. (2002). A data brief on the Smithsonian abyssal volcanic glass data file. Geochemistry, Geophysics, Geosystems 3(4), 1023.
- Millen, D. W. & Hamburger, M. W. (1998). Seismological evidence for tearing of the Pacific plate at the northern termination of the Tonga subduction zone. Geology 26(7), 659-662.
- Min, K., Mundil, R., Renne, P. R. & Ludwig, K. R. (2000). A test for systematic errors in 40Ar/39Ar geochronology through comparison with U/Pb analysis of a 1.1-Ga rhyolite. Geochimica et Cosmochimica Acta 64(1), 73-98.
- Morgan, W. J. (1971). Convection plumes in the lower mantle. Nature 230(5288), 42-43.
- Morgan, W. J. (1972). Deep mantle convection plumes and plate motions. AAPG Bulletin 56(2), 203-213.
- Nakamura, Y. & Tatsumoto, M. (1988). Pb, Nd, and Sr isotopic evidence for a multicomponent source for rocks of Cook-Austral Islands and heterogeneities of mantle plumes. Geochimica et Cosmochimica Acta 52(12), 2909-2924.
- Natland, J. H. (1980). The progression of volcanism in the Samoan linear volcanic chain. American Journal of Science 280, 709-735.
- Natland, J. H. (2003), The Samoan Chain: A Shallow Lithospheric Fracture System. http://www.mantleplumes.org/Samoa.html
- Natland, J. H. & Turner, D. L. (1985). Age progression and petrological development of Samoan shield volcanoes: evidence from K-Ar ages, lava compositions, and mineral studies. Investigations of the Northern Melanesian Borderland, Circum-Pacific Council for Energy and Mineral Resources. Earth Science Series, Vol. 3. pp. 139-171. Circum-Pacific Council for Energy and Mineral Resources, Houston, Texas.
- Oulton, J., Humayun, M., Fedkin, A. & Grossman, L. (2016). Chemical evidence for differentiation, evaporation and recondensation from silicate clasts in Gujba. Geochimica et Cosmochimica Acta 177, 254-274.
- Pearce, J. A., Kempton, P. D. & Gill, J. B. (2007). Hf-Nd evidence for the origin and distribution of mantle domains in the SW Pacific. Earth and Planetary Science Letters 260(1-2), 98-114.
- Pelletier, B. & Auzende, J. M. (1996). Geometry and structure of the Vitiaz trench lineament (SW Pacific). Marine Geophysical Researches **18**(2), 305-335.
- Phipps Morgan, J., Morgan, W. J., Zhang, Y. S. & Smith, W. H. (1995). Observational hints for a plume-fed, suboceanic asthenosphere and its role in mantle convection. Journal of Geophysical Research: Solid Earth 100(B7), 12753-12767.
- Poreda, R. J. & Farley, K. A. (1992). Rare gases in Samoan xenoliths. Earth and Planetary Science Letters 113(1-2), 129-144.
- Price, A. A., Jackson, M. G., Blichert-Toft, J., Hall, P. S., Sinton, J. M., Kurz, M. D. & Blusztajn, J. (2014). Evidence for a broadly distributed Samoan-plume signature in the northern Lau and North Fiji basins. Geochemistry, Geophysics, Geosystems 15, 986-1008.
- Price, A. A., Jackson, M. G., Blichert-Toft, J., Blusztajn, J., Conatser, C. S., Konter, J. G., Koppers, A. A. & Kurz, M. D. (2016). Geochemical evidence in the northeast Lau Basin for subduction of the Cook-Austral volcanic chain in the Tonga trench. Geochemistry, Geophysics, Geosystems 17, 1694-1724.
- Price, A. A., Jackson, M. G., Blichert-Toft, J., Kurz, M. D., Gill, J., Blusztajn, J., Jenner, F., Brens, R. & Arculus, R. (2017). Geodynamic implications for zonal and meridional isotopic patterns across the northern Lau and North Fiji basins. Geochemistry, Geophysics, Geosystems 18(3), 1013-1042.
- Price, R. C., Maillet, P., McDougall, I. & Dupont, J. (1991). The geochemistry of basalts from the Wallis Islands, northern Melanesian Borderland: evidence for a lithospheric origin for Samoan-type basaltic magmas? Journal of Volcanology and Geothermal Research 45(3), 267-288.

- Regelous, M., Turner, S., Falloon, T. J., Taylor, P., Gamble, J. & Green, T. (2008). Mantle dynamics and mantle melting beneath Niuafo'ou island and the northern Lau back-arc basin. Contributions to Mineralogy and Petrology 156(1), 103–118.
- Reinhard, A. A., Jackson, M. G., Koornneef, J. M., Rose-Koga, E. F., Blusztajn, J., Konter, J. G., Koga, K. T., Wallace, P. J. & Harvey, J. (2018). Sr and Nd isotopic compositions of individual olivine-hosted melt inclusions from Hawai'i and Samoa: implications for the origin of isotopic heterogeneity in melt inclusions from OIB lavas. Chemical Geology 495, 36-49.
- Reinhard, A. A., Jackson, M. G., Blusztain, J., Koppers, A. A., Simms, A. R. & Konter, J. G. (2019). "Petit spot" rejuvenated volcanism superimposed on plume-derived Samoan shield volcanoes: evidence from a 645-m drill core from Tutuila Island, American Samoa. Geochemistry, Geophysics, Geosystems 20(3), 1485-1507.
- Rose, J. & Koppers, A. A. (2019). Simplifying age progressions within the Cook-Austral Islands using ARGUS-VI high-resolution 40Ar/39Ar incremental heating ages. Geochemistry, Geophysics, Geosystems 20(11), 4756-4778.
- Ruellan, E., Delteil, J., Wright, I. & Matsumoto, T. (2003). From rifting to active spreading in the Lau Basin–Havre Trough backarc system (SW Pacific): Locking/unlocking induced by seamount chain subduction. Geochemistry, Geophysics, Geosystems 4(5), 8909. https:// doi.org/10.1029/2001GC000261.
- Salters, V. J., Mallick, S., Hart, S. R., Langmuir, C. E. & Stracke, A. (2011). Domains of depleted mantle: new evidence from hafnium and neodymium isotopes. Geochemistry, Geophysics, Geosystems **12**(8).
- Sinton, J. M., Johnson, K. T. M., & Price, R.C. (1985). Petrology and geochemistry of volcanic rocks from the Northern Melanesian borderland. Investigations of the Northern Melanesian Borderland, Circum-Pacific Council for Energy and Mineral Resources. Earth Science Series, Vol. 3, pp. 35-65. Circum-Pacific Council for Energy and Mineral Resources, Houston, Texas.
- Staudigel, H., Hart, S. R., Koppers, A. A., Constable, C., Workman, R., Kurz, M. & Baker, E. T. (2004). Hydrothermal venting at Vailulu'u seamount: the smoking end of the Samoan chain. Geochemistry, Geophysics, Geosystems 5(2), Q02003. https://doi.org/10.1029/2003 GC000626.
- Staudigel, H., Hart, S. R., Pile, A., Bailey, B. E., Baker, E. T., Brooke, S., Connelly, D. P., Haucke, L., German, C. R., Hudson, I. & Jones, D. (2006). Vailulu'u seamount, Samoa: life and death on an active submarine volcano. Proceedings of the National Academy of Sciences of the United States of America 103(17), 6448-6453.
- Tanaka, T., Togashi, S., Kamioka, H., Amakawa, H., Kagami, H., Hamamoto, T., Yuhara, M., Orihashi, Y., Yoneda, S., Shimizu, H. & Kunimaru, T. (2000). JNdi-1: a neodymium isotopic reference in consistency with LaJolla neodymium. Chemical Geology 168(3-4), 279-281.
- Turner, D. L. & Jarrard, R. D. (1982). K-Ar dating of the Cook-Austral island chain: a test of the hot-spot hypothesis. Journal of Volcanology and Geothermal Research 12(3-4), 187-220.
- Turner, S. & Hawkesworth, C. (1998). Using geochemistry to map mantle flow beneath the Lau Basin. Geology 26(11), 1019–1022.
- Weis, D., Kieffer, B., Maerschalk, C., Barling, J., De Jong, J., Williams, G. A., Hanano, D., Pretorius, W., Mattielli, N., Scoates, J. S. & Goolaerts, A. (2006). High-precision isotopic characterization of USGS reference materials by TIMS and MC-ICP-MS. Geochemistry, Geophysics, Geosystems 7(8), Q08006. https://doi.org/10.1029/2006
- Weis, D., Kieffer, B., Hanano, D., Nobre Silva, I., Barling, J., Pretorius, W., Maerschalk, C. & Mattielli, N. (2007). Hf isotope compositions of US Geological Survey reference materials. Geochemistry,

- Geophysics, Geosystems 8, Q06006. https://doi.org/10.1029/2006 GC001473.
- Wendt, J. I., Regelous, M., Collerson, K. T. & Ewart, A. (1997). Evidence for a contribution from two mantle plumes to island-arc lavas from northern Tonga. Geology 25(7), 611-614.
- Wessel, P. & Kroenke, L. W. (2008). Pacific absolute plate motion since 145 Ma: an assessment of the fixed hot spot hypothesis. Journal of Geophysical Research 113, B06101.
- White, W. M., Albarède, F. & Télouk, P. (2000). High-precision analysis of Pb isotope ratios by multi-collector ICP-MS. Chemical Geology **167**(3-4), 257-270.
- Woodhead, J. D. & Hergt, J. M. (2000). Pb-isotope analyses of USGS reference materials. Geostandards Newsletter 24(1), 33-38.
- Workman, R. K. & Hart, S. R. (2005). Major and trace element com-

- position of the depleted MORB mantle (DMM). Earth and Planetary Science Letters 231(1-2), 53-72.
- Workman, R. K., Hart, S. R., Jackson, M., Regelous, M., Farley, K. A., Blusztajn, J., Kurz, M. & Staudigel, H. (2004). Recycled metasomatized lithosphere as the origin of the enriched mantle II (EM2) end-member: evidence from the Samoan volcanic chain. Geochemistry, Geophysics, Geosystems 5, Q04008.
- Wright, E. & White, W. M. (1987). The origin of Samoa: new evidence from Sr, Nd, and Pb isotopes. Earth and Planetary Science Letters 81(2-3), 151-162.
- Zhang, H., Yan, O., Li, C., Zhu, Z., Zhao, R. & Shi, X. (2019). Geochemistry of diverse lava types from the Lau Basin (South West Pacific): implications for complex back-arc mantle dynamics. Geological Journal **54**(6), 3643-3659.